Magnetization, Magnetostriction and Thermal Expansion of Fe-Ni alloy System

By

A. S. M. SIRAJUL ISLAM

A Thesis Presented to the Department of Physics, BUET, Dhaka
in partial fulfillment of the requirements for the degree of M.Phil

Bangladesh University of Engineering & Technology
Dhaka, Bangladesh
November 1995

BANGLADESH UNIVERSITY OF ENGINEERING & TECHNOLOGY

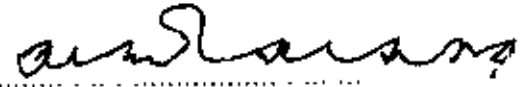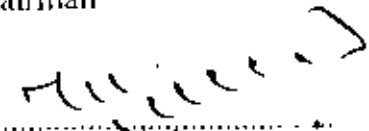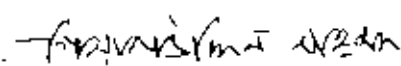## DEPARTMENT OF PHYSICS

CERTIFICATION OF THESIS WORK
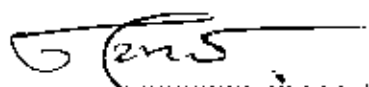
A THESIS ON

Magnetization, Magnetostriction and Thermal Expansion of Fe-Ni Alloy System

BY
A. S. M.SIRAJUL ISLAM

has been accepted as satisfactory in partial fulfilment for the degree of Master of Philosophy in Physics and certify that the student demonstrated a satisfactory knowledge of the field covered by this thesis in an oral examination on 30th November 1995.

BOARD OF EXAMINERS

1. Prof. M. Ali Asgar (Supervisor)
   Department of Physics
   BUET. Dhaka

   Chairman

2. Dr. Mominul Huq (Co-Supervisor)
   Department of Physics
   BUET. Dhaka

   Member

3. Prof. Gias uddin Ahmad
   ι Head, Department of Physics
   BUET, Dhaka.

   Member

4. Prof. Tafazzal Hossain
   Department of Physics
   BUET, Dhaka.

   Member

5. Prof. M. Ibrahim
   Department of Physics
   Dhaka University. Dhaka.

   Member

CERTIFICATE

This is to certify that this thesis which I have presented for an M.Phil degree embodies the results of my course of further study and research and that this work has not been submitted elsewhere for the award of any degree or diploma.

(A. S. M. Sirajul Islam)
Candidate

(Dr. M. Ali Asgar)
Professor
Department of Physics
BUET, Dhaka

Supervisor

(Dr. Mominul Huq)
Associate Professor
Department of Physics
BUET, Dhaka

Co-Supervisor

ACKNOWLEDGEMENT

ABSTRACT

As a part of Invar problem magnetization, magnetostriction and thermal expansion of Fe-Ni alloys have been measured. Fe-Ni alloys of the composition $Fe_{100-x}Ni_x$ (where x = 30, 35, 40, 45, 50 and 78) are prepared by powder technique, using induction furnace. It is thus possible to prepare the alloys with a sintering temperature below the melting points of the constitutent element. The sintered samples are annealed in a furnace at a temperature of 1000°C for 15 hours. X-ray photographs are also used for the characterisation of the alloys. From the microstructures of the alloys, their homogencity and grain boundaries are examined.

Field and composition dependence of magnetization of the alloy system are measured using a vibrating sample magnetometer. Linear increase of the saturation magnetization is observed with increasing iron concentration upto 65 at% of iron. This result is explained by using localized model. The saturation magnetization, however, is observed to decrease abruptly, around 70 at% of Fe, which is explained by assuming antiferromagnetic coupling between iron atoms, although the exchange interaction between iron and nickel atoms and between nickel atoms remain positive.

The saturation magnetostriction as well as the field dependence of magnetostriction of the different alloy compositions are measured and the results are explained in terms of the conventional theories of magnetostriction. A relation between magnetization and magnetostriction is obtained from the experimental results and is explained in terms of 180° domain wall movement and 90° domain rotation.

Thermal expansion of $Fe_{60}Ni_{40}$ alloy is measured using strain gauge technique. The slight anomally observed around 250°K is explained as due to unequal contributions from thermal expansion and volume magnetostriction at this composition.

(iii)

CONTENTS

REFERENCE

CHAPTER 1   INTRODUCTION

Fe-Ni alloy system is one of the most studied magnetic alloys. This is partly due to its numerous applications and partly due to complex and interesting magnetic properties. The measurement of magnetization and the study of its variation with magnetic field are important for the understanding and characterization of Fe-Ni alloys.

In Fe-Ni alloys, since the component metals have opposite magnetostriction, it is expected that an appropriate composition will give rise to the desired result of zero magnetostriction and low thermal expansion. Some work on anomalous thermal expansion of some Fe-Ni alloys have already been investigated and the lattice contribution to thermal expansion has been calculated.

There is an enormous interest in materials with zero thermal expansion and high magnetic permeability due to their technological importance. Ch. E. Guillaume[2] found, in 1897, that ferromagnetic fcc FeNi alloys at concentrations around $Fe_{65}Ni_{35}$ show almost constant invariant thermal expansion as a function of temperature in a wide range around room temperature. This was termed as invar effect. The original work by Guillaume was the basis for wide spread experimental and theoretical activities in the 1950s and 1960s especially in Japan[24-34] and Europe[4-23], and with increasing understanding of Solid State Magnetism, the number of publications about Invar and Invar-related topics increased

dramatically. The reason for this increase was two-fold. First, the observation of Invar anomalies extended beyond to ferromagnetic fcc FeNi alloys and Invar anomalies are observed in ferromagnetic as well as antiferromagnetic binary, ternary alloys systems. The lattice structure is of no influence, and Invar systems can have fcc, bcc, hexagonal and other structures or even be amorphous. Moreover, Invar anomalies are observed in rare earth transition metal compounds with Lavesphase structure. The key point is that the systems are rich in at least one 3d-transition element. There are no purely 4f Invar alloys or compounds. This shows that the Invar effect is obviously a problem of itinerant 3d-magnetism.

Secondly, although the name Invar resulted from the anomaly in the thermal expansion, a broad variety of physical anomalies now have been known to be associated with Invar problem. The main physical properties in which Invar anomalies are observed, as a function of composition and variable external parameters like temperature, magnetic field and pressure are thermal expansion, lattice constant, spontaneous volume magnetostriction, heat capacity, magnetization and pressure. Recent updating on the physical understanding of Invar have been reported by Wassermann(1987, 1988, 1989)[38,39,40] and in the proceedings of the International symposium on Magneto-elasticity and Electronic Structure of Transition Metals, Alloys and Films, which took place in spring 1989 in Duisburg, FRG.

Although the term Invar initially stood for alloys showing minimum thermal expansion coefficients associated with maximum spontaneous volume

magnetostriction in certain ranges of composition and temperatures, the term Invar is now extended in its meaning to include many more observed anomalies.It is therefore, suggested that a more general headline, summarizing all the features would be moment-volume instabilities in 3d-transition element rich system.

In order to understand the Invar effect in 3d-transition metal alloys, there have been two different basic approaches. One is based on the localized electron picture (Heisenberg model)[20,52] in which each atom has its own permanent and temperature independent moment and are considered localised at the respective atomic sites. The other is based on the itinerant picture of magnetism (Stoner model)[23] where the magnetic electrons are treated as waves belonging to the whole crystal, to explain the composition dependence of the average moment (Slater-Pauling curve)[43,44]. This has the drawback that the band splitting vanishes at T_c which is, as we have seen, not the case in Invar. The early local models stressed the metallurgical and/or magnetic inhomogeneity as Invar relevance, since in the archetypical Invar system FeNi the magnetovolume effects reach a maximum near the $\gamma-\alpha$ transition at $Fe_{65}Ni_{35}$, where simultaneously a strong deviation of the average magnetic moment from the Slater-Pauling curve was observed. By now more than 20 different models for the understanding of the Invar effect has been published. The most important ones are 'model of latent antiferromagnetism' (Kondorsky and Sedov 1960, Jo 1976) [8,31], the 'local models with different short-range order (Sidorov and Doroshenko 1966, Dubinin et at. 1971)[7,20] the 'local environment models' (Schlösser 1971, Kanamori 1974) [35,51], the 'inhomogeneity models' (Kachi and Asano 1969 Shimizu 1979) [29,50] as well as 'Zener-type model' (Colling and Car 1970) [4]. However, with the detection of

3

the Invar effect on ordered Fe$_3$Pt, a system which neither shows mixed magnetic behaviour nor deviation of the average moment from the Stater-Pauling curve, all these models come principally in to doubt [41]. This only proves that more of experimental investigation is needed to come to a fuller understanding of the problem. The present work is expected to contribute in this respect.

The major fields for technical applications of these type of bi-metals, are wires for printers and x-y recorders, liquid natural gas (LNG) tanks and pipelines, precision machine tools, precision pendulums, precision capacitors, precision moulds, transistor bases, lead frames for integrated circuits, membranes, springs, glass (ceramic)-metal seals, pressure gauge, thermostats, bending meters, gravity meters, flow meters, astronomical telescopes, seismographic devices, microwave guides, resonant cavities, laser light sources, radar echo boxes.

Although some materials with very low thermal expansion and high permeability are available commercially, their composition and the preparation techniques are usually not disclosed. There is also a great interest for understanding the mechanism responsible for these unusual properties.

The temperature dependence of the anharmonicity of the lattice vibration determining thermal expansion and the magneto-elastic interaction responsible for magnetostriction have a critical balance in some magnetic alloys over a temperature range. The understanding of this mechanism is essential in finding alloys with special properties like high permeability and zero thermal expansion.

The aim of this thesis is the preparation of iron-nickel alloys of different composition and the investigation of the magnetization, magnetostriction and thermal expansion of this ferromagnetically ordered alloy system.

The field required to magnetize ferromagnetic substances are considerably weaker than those required for paramagnetics. The atomic magnetic moments in a ferromagnetic substance interact strongly with one another and tend to align themselves parallel to each other. The interaction is such as to correspond to an applied field of the order of magnetude 10^9 A/m and it results in a nearly perfect alignment of the spins inspite of the thermal agitation at room temperature. The presence of a strong internal magnetic field was first postulated by P.Weiss[45]. He called it the molecular field and developed a theory of the temperature dependence of the saturation magnetization, which is described in chapter (2.1). The physical origin of the molecular field was not understand until 1928, when Heisenberg showed that it was caused by quantum-mechanical exchange forces. The atomic moments of the magnetic materials originates from the orbital motion and the spin motion of the electrons of the unfilled 3d atomic shells. The magnitude of the moment depends on the coupling of the orbital & spin anguler momentum.

The physical origin of magnetostriction and magnetoelastic co-efficients is explained from phenomenological and thermodynamic consideration.

Magnetostriction originates in the interaction between the atomic magnetic moments and is closely related to magnetic anisotropy and plays an important role in the understanding of ferromagnetic and antiferromagnetic phenomena like magnetization process[42]. The theoretical understanding of the magnetostriction is described in chapter (2.3). Studies of magnetostriction also have technological utility in the production of electromechanical transducers, magnetostrictive oscillators and filters and in removing transformer noises caused by magnetostrictive vibrations of the core.

The preparation technique of Fe-Ni alloys from powder technology, sintering process and study of metallography are described in chapter (3). Iron and Nickel powder in appropriate atomic percentage are mixed with morter and pestle for each composition. This mixed powder sample is pressed into the required form in a die using a perssing machine. The pressed sample is sintered in a furnace. The sintering process is usually carried out at a temperature below the highest melting points of the constituents. The X-ray photographs are also used to detect α-phase and γ-phase precipitation, Which could just barely be seen in the photographs of some of the sample.

There are various methods for the measurement of magnetization. An advanced type of apparatus, the vibrating sample magnetometer developed by S. Foner [46,47] is used in our experiment for measuring magnetization of Fe-Ni alloys with compositions $Fe_{100-x}Ni_x$ (where x = 30, 35, 40, 45, 50 and 78) at room temperature of 300°K.. The sample is cemented to the end of a rod and the other end of

which is fixed to a loudspeaker. The specimen is vibrated in a vertical direction by flowing current through the loudspeaker. The ac signal induced by the dipole field of the specimen in a pair of secondary coils placed on both sides of the specimen is amplified and compared with a signal produced by a standard magnet, giving rise to an output signal which is exactly proportional to the magnetic moment of the specimens. This is described in chapter (4.1).

The linear increase of the saturation magnetization in iron-nickel alloys with increasing iron concentration is explained using localized model by Friedel[48]. The sudden decrease of the saturation magnetization in iron-nickel alloys around 30 at% Ni is explained using the localized moment model assuming negative iron-iron nearest neighbour exchange interaction and also by itinerant electron theory. This is explained in chapter (4.2).

The straingauge technique has been used successfully for measurements of magnetostriction of the Fe-Ni alloys at room temperature. This method was first introduced by Goldman[49] and has since then become increasingly popular for its simplicity, compactness and precision. A convenient method of determining change in length is to measure the change in resistance of a wire of the strain gauge that is firmly cemented to the test specimen and expands and contracts with it. A d.c. wheat stone bridge in slightly out of balance condition is used to measure the fractional change in resistance in the active gauge. The deflection observed in the nanovoltmeter which is connected to the wheatstone bridge circuit is used as a measure of the strain. There is a linear relationship between the deflection of the nanovoltmeter and fractional change in resistance. This is described in chapter (5.1).

Measurements of magnetostriction of Fe-Ni alloys with different concentrations at room temperature have been reported in chapter (5.2). The magnetostriction of Fe-Ni alloys of the composition Fe_{100-x} Ni_x (where x = 30, 35 and 40) are plotted against the intensity of magnetization. When the magnetization approaches saturation, the magnetostriction also approaches its limiting value, λ_s, the saturation magnetostriction.

The thermal expansion of Fe_{60} Ni_{40} alloy has been investigated and explained in chapter(6). Low thermal expansion is responsible for a large spontaneous volume magnetostriction which cancels a normal lattice expansion resulting in the near-zero net expansion in a broad temperature range centered on room temperature.

CHAPTER 2   THEORIES OF FERROMAGNETISM

2.1.   State of Ferromagnetism

The first successful theory to explain ferromagnetism was put forward by P.Weiss[1] in 1907. He introduced two basic concepts to explain ferromagnetic ordering. These are the existence of a molecular field which is proportional to magnetization of the sample and the existence of domains which are region of spontaneous homogeneous magnetization. This theory is in a way, an extension of the classical theory of paramagnetism which was developed by Langevin assuming each atomic moment as a non-interacting independent entity. The magnetic field requirement for paramagnetic materials to reach saturation is of the order of 10^9 A/m.

On the other hand, the field required to magnetize a ferromagnetic substance, such as supermally to saturation can be as small as 1 A/m, while the field required for alnico is about 5×10^4 A/m. Most of the ferromagnetic materials can be saturated by a magnetic field whose intensity lies between these two values. Thus the magnetic fields needed to magnetize a ferromagnetic substance is considerably weaker than those required for paramagnetic materials. According to this picture the atomic magnetic moments in a ferromagnetic substance interact strongly with one another and tend to align themselves parallel to each other. The interaction is such as to correspond to an applied field of the order of magnitude as large as 10^9 A/m and it causes in a nearly perfect alignment of the spins inspite of the thermal agitation at room temperature[2]. The effect of an externally applied field is merely to change the direction of the spontaneous magnetization.

9

If we consider a substance in which each atom has a net magnetic moment M. of n spins, then

$$M = n \, \mu_B \tag{1}$$

Each atomic moment is assumed to be acted on by the molecular field, which is proportional to the magnetization of its environment. Classically the field should be given by the Lorentz field, which is given by

$$H = 1/3\mu_3 \tag{2}$$

However, the molecular field is not the classically Lorentz field, but an exchange field of Quantum mechanical orgin. We can express the molecular field as,

$$H_m = w \, I \tag{3}$$

where w is the proportionality factor.

Now, if a magnetic field H is applied parallel to the magnetization I of the system, an individual atomic moment has the potential energy

$$U_E = - \, M(H + wI) \, Cos\theta \tag{4}$$

Since the probability for an atomic moment to have this energy is proportional to the Boltzman factor $e^{-U_E/KT}$ the average magnetization is given by

$$I = NM \frac{\int_0^\pi e^{M(H + wI)Cos\theta/Kt} . \, Cos\theta . \, Sin\theta . d\theta}{\int_0^\pi e^{M(H + wI)Cos\theta/KT} . \, Sin\theta . d\theta}$$

$$\text{or } I = NML \, [M \frac{(H+wI)}{KT}] \tag{5}$$

If we set the argument of the Langevin function equal to a

we have $I = NML(a)$ (6)

and from the definition of a,

$$I = \frac{aKT}{Mw} - \frac{H}{w} \tag{7}$$

In fig. (2.2a) we have a graphical representation of equation (6) and eqn (7).

10
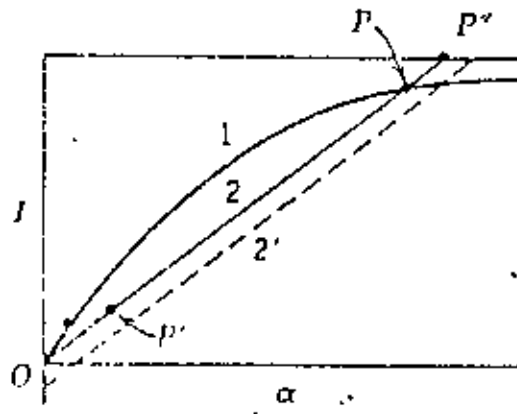
Fig. 2.2a : Graphical representation of equation (6) and (7).
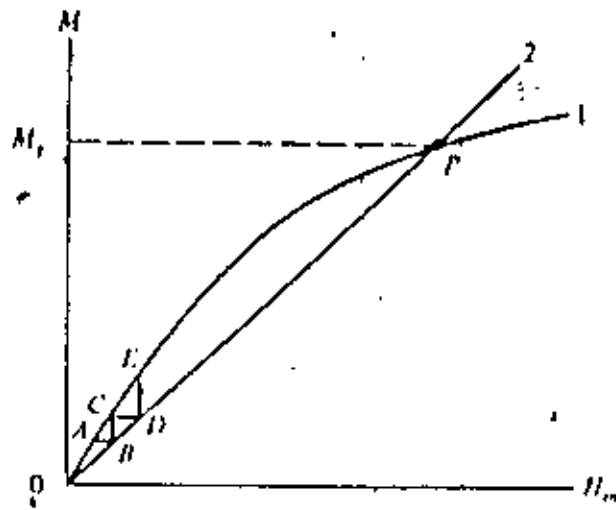
Fig. 2.2b : Spontaneous Magnetization of molicular field.

Curve-1 represents the Langevin function and curve-2, a straight line through the origin, represents eqn. (7) for H = O. The magnetization I, which the molecular field will produce in the material is given by the intersection points of this two curves. There are actually two intersections one at the origin O and the other at the point P. The actual stable solution is given by the point P, where as the other intersection point O corresponds to an unstable solution[2]. The later point represents the state for which I=O, the state in which there is a random distribution of the directions of the atomic moments.

If a small field is applied on the material, it will be magnetized to the point A (say) But if I = A, then the line 2 states that H_m is B. But a field of this strength would produce a magnetization represented by the point C in the curve(2.2b). Thus I would go through the values of O,A,C,E .... and arrive at P. Now P is a point of stability, because the magnetization greater than P will spontaneously revert to P, in the absence of an applied field.

We shall now discuss how this behaviour is affected by changes in temperature and how I_s will vary with temperature and at what temperature the material will become paramagnetic. We now replot fig. (2.2b) with a as a variable rather than H_m where

$$a = \frac{M(H + H_m)}{KT}$$

When the applied field is zero, We have

$$a = \frac{MwI}{KT} = \frac{MwII_0}{KTI_0} \tag{8}$$

$$\text{or} \quad \frac{I}{I_0} = \left(\frac{KT}{MwI_0}\right) a \tag{9}$$

$\dfrac{I}{I_0}$ is a linear function of a with a slope proportional to the absolute temperature. In fig (3) curve-1 is the Langevin function and line-2 is a plot of eqn. (9) for a temperature T_2. Their intersection at P gives the spontaneous fractional magnetization $\dfrac{I_s}{I_0}$ achieved at this temperature. An increase in temperature above T_2 has the effect of rotating line- 2 counterclockwise about the origin. This rotation causes P and the corresponding magnetization to move lower and lower on the Langevin curve. The spontaneous magnetization vanishes at temperature T_3 when the line is in position 3, tangent to the Langevin curve at the origin, T_3 is therefore equal to the curie temperature T_c. At any higher temperature, such as T_4 the substance is paramagnetic, because it is not spontaneously magnetized[3].

The curie temperature can be evaluated from the fact that slope of line 3 is the same as the slope of the Langevin curve at the origin, which is $\dfrac{1}{3}$. Replacing T with T_c

We have

$$\frac{KT_c}{MwI_0} = \frac{1}{3}$$

$$\text{or} \quad T_c = \frac{MwI_0}{3K} \tag{10}$$

13
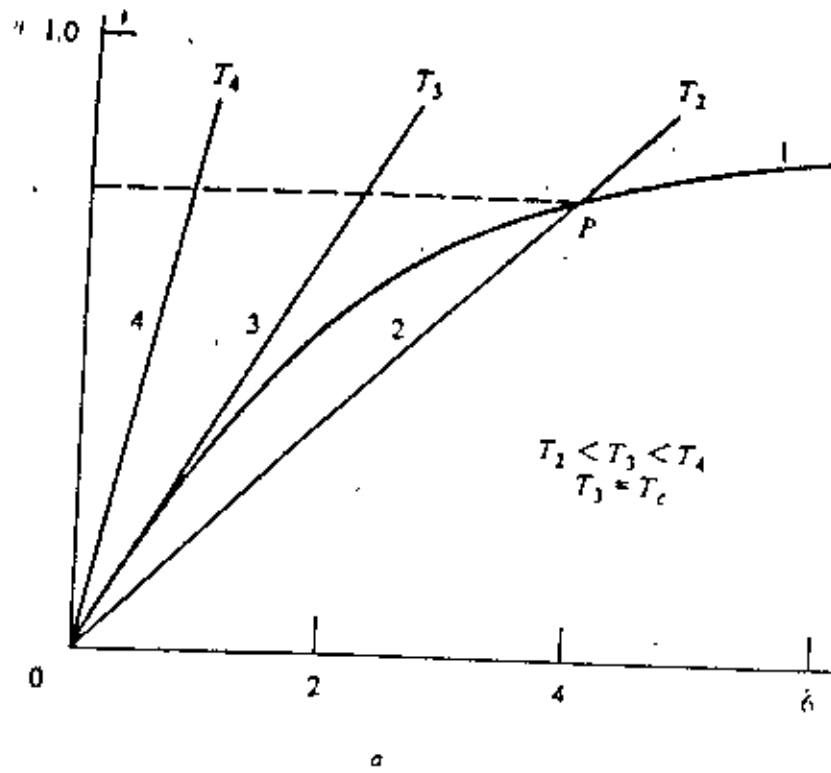
Fig. 2.3 : Effect of temperature on spontaneous Magnetization

14

Therefore the slope of the straight line representing the molecular field is, at any temperature,

$$\frac{KT}{Mw i_0} = \frac{T}{3T_c} \tag{11}$$

But the slope of the line determines the point of intersection P with the Langevin curve and hence the value of $\frac{I_s}{i_0}$. Therefore $\frac{I_s}{I_0}$ is determined solely by the ratio $\frac{T}{T_c}$. This means that all ferromagnetic materials, which naturally have different values of I_0 and T_c have the same value of $\frac{I_s}{I_0}$ for any particular value of $\frac{T}{T_c}$. This is sometimes called the law of corresponding states.

If we then define, for a ferromagnetic material, σ_s and σ_0 as the saturation magnetizations at $T°K$ and $0°K$ respectively an exact statement of the law of corresponding states is that all the materials have the same value of $\frac{\sigma_s}{\sigma_0}$ for the same Value of $\frac{T}{T_c}$. The relation between the σ and I values is

$$\frac{\sigma_s}{\sigma_0} = \frac{I_s/\rho_s}{I_0/\rho_0} = \frac{I_s \rho_0}{I_0 \rho_s} \tag{12}$$

Where ρ_s and ρ_0 are the densities at $T°K$ and $0°K$, respectively.

A change from I to σ also involves a change in the molecular field constant ω.

$$H_m = wI = w\rho(\frac{I}{\rho}) = (w\rho)\sigma \tag{13}$$

Thus $(w\rho)$ becomes the molecular field constant.

15

Then from equation (10) we have

$$T_c = \frac{M\omega p\sigma_0}{3K}$$

and from equation (11), we have

$$\frac{KT}{Mw p\sigma_0} = \frac{T}{3T_c} \tag{14}$$

Equation (9) therefore becomes

$$\frac{\sigma}{\sigma_0} = (\frac{KT}{Mwp\sigma_0})a = (\frac{T}{3T_c})\, a \tag{15}$$

when the magnetization is expressed in terms of σ

The Weiss theory is modernized by supposing that the molecular field acts on a substance having a relative magnetization determined by a quantum mechanical Brillouin function $B_J(a)$, in terms of specific magnetization we have

$$\frac{\sigma}{\sigma_0} = \frac{2J+1}{2J} \text{Cot h}(\frac{2J+1}{2nJ})\, a - \frac{1}{2J} \text{Cot h}\frac{a}{2J} \ldots \tag{16}$$

where $a = \frac{M(H + wI)}{KT} = \frac{gJ\mu_\beta(H + wI)}{KT}$

The straight line representing the molecular field is given by

$$\frac{\sigma}{\sigma_c} = \frac{KT}{(Mwp\sigma_0)}\, a \tag{17}$$

16

The slope of the Brillouin function at the origin is

$$\frac{J + 1}{3J}$$

Therefore, the curie temperature is

$$T_c = \left(\frac{Mw\rho\sigma_0}{K}\right) \times \frac{J + 1}{3J} \tag{18}$$

$$= \left(\frac{gJ\mu_B w\rho\sigma_0}{K}\right) \times \frac{J + 1}{3J}$$

$$= \frac{g(J + 1)\mu_B w\rho\sigma_0}{3K} \tag{19}$$

The equation of the molecular field line can then be written

$$\frac{\sigma}{\sigma_0} = \left(\frac{J + 1}{3J}\right) \times \left(\frac{T}{T_c}\right)a \tag{20}$$

values of the relative spontaneous magnetization $\dfrac{\sigma_s}{\sigma_0}$ as a function of $\dfrac{T}{T_c}$ can be found graphically from the intersections of the curve of eqn. (16) and the line of equation (20).

.2.2 Intrinsic Magnetization of Alloys

Almost all magnetic alloys contain at least one of the three ferromagnetic metals Iron, cobalt or nickel which exhibit ferromagnetism at room temperature. By alloying these metals with other elements, we can prepare magnetic substances

17

which have various magnetic properties. The properties of magnetic materials depend on chemical composition, fabrication and heat treatment. These properties are mainly determined by the magnetic anisotropy, magnetostriction and secondary structure of the substances. The intrinsic magnetization of an alloy is determined by its electronic structure.

On the basis of an elementary knowledge of atomic structure two possible origins are proposed for the atomic magnetic moment. One of these is the orbital motion of the electron around the nucleus and the other is a spin motion of the electron about its own axis. Ferromagnetism has its origin in the spin and orbital magnetic moments in an unfilled electron shell. Each of the three ferromagnetic elements Fe, Co, Ni has an unfilled 3d shell. Variation of atomic magnetic moment in these materials with the number of electrons in the (3d + 4s) shells is shown graphically in fig (2.4). This curve is usually referred to as the Slater-Pauling curve [20,21]. The average atomic magnetic moments of various alloys depend only on the number of electrons per atom. This is reasonable when the alloying atoms are only one or two atomic numbers aparts, as in the series Ni-Cu and Fe-Ni alloy.

Most of the alloys are represented by points falling on a curve consisting of two straight lines. One of these lines rises from 0 Bohr magnetons at Cr at the rate of about $1\mu_B$ per electron, while the other falls from $2.5\mu_B$ at about 30 at% Co-Fe at the rate of about $-1\mu_B$ per electron. We have seen that ferromagnetism, in 3d-transition metals appears for average electron concentration ranging from 24 to 28.6. Since the argon shell ($1s^2\ 2s^2\ 2P^6\ 3s^2\ 3P^6$) is filled by 18 electrons, the

18

number of 3d and 4s electrons in these ferromagnetic alloys ranges from 6 to 10.6. If we assumed that the number of conduction electrons is about 1.0 at Cr and 0.6 at Ni, the number of 3d electrons is then 5 to 10 in the range where ferromagnetism is realized.

In order to explain the appearance of ferromagnetism it is essential to identify the physical origin of the molecular field proposed by Weiss, which gives rise to the parallel alignment of spins. The accepted interpretation of the nature of the molecular field as presented by Heisenberg [5] in 1928 is quantum mechanical in origin.

For a particular pair of atoms, situated at a certain distance apart, as in the case of a hydrogen molecule there are certain electrostatic attractive forces between the electrons and protons and repulsive forces between the two electrons and between the two protons. These can be calculated by Coulomb's law. But there is still another force, ·entirely non-classical, which depends on the relative orientation of the spins of the two electrons. This is the exchange force. If the spins are antiparallel, the sum of all the forces is attractive and a stable molecule is formed. The total energy of the atoms is then less for a particular distance of separation than it is for smaller or larger distances. If the spins are parallel, the two atoms repel one another. The exchange force is a consequence of the Pauli's exclusion principle applied to the two atoms as a whole. This principle states that two electrons can have the same energy only if they have opposite spins. If their spins are parallel, the two electrons will tend to stay far apart. The ordinary (coulomb) electrostatic energy is therefore modified by the
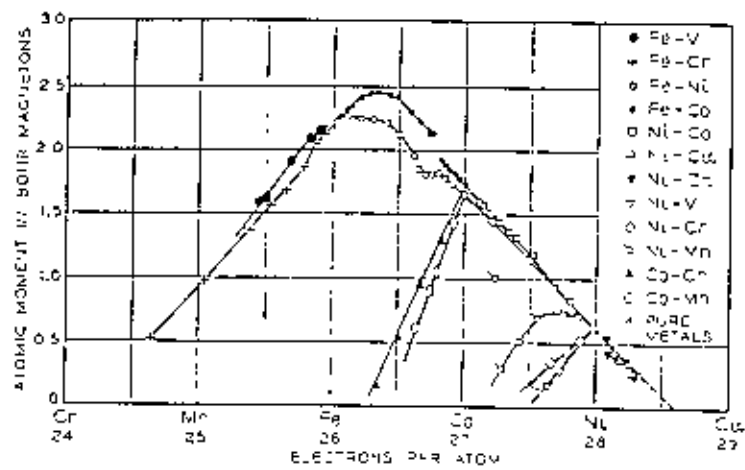
Fig. 2.4 : Slater-Pauling curve

spin orientations. This means that the exchange force is fundamentally electrostatic in origin. The term "exchange" arises in the following way. When the two atoms are adjacent, we can consider electron 1 moving about proton 1 and electron 2 moving about proton 2, But the electrons are indistinguishable, and we must also consider the possibility that the two electrons exchange places, so that electron 1 moves about proton 2 and electron 2 about proton 1. This consideration introduces an additional term, the exchange energy, into the expression for the total energy of the two atoms. This interchange of electrons takes place at a very high frequency about 10^{18} times per second in the hydrogen molecule.

The exchange energy forms an important part of the total energy of many molecules and of the covalent bond in many solids. Heisenberg showed that it plays a decisive role in ferromagnetism. If two atoms i and j have spin angular momentum S_i and S_j respectively, then the exchange energy between them is given by

$$E_{ex} = -2J_{ex} \; S_i . S_j$$
$$= -2J_{ex} \; S_i . S_j Cop\varphi \tag{1}$$

Where J_{ex} is called the exchange integral and ϕ is the angle between the spins. If J_{ex} is positive, E_{ex} is a minimum when the spins are parallel ($\cos\phi = 1$) and a maximum when they are antiparallel ($\cos\phi = -1$).

When we stem from a hydrogen molecule to a ferromagnetic crystal calculation of J_{ex} becomes formidable. Equation [1] which is itself something of a simplification and which applies only to two atoms, have to be summed over all the atom pairs

in the crystal. Exchange forces decrease rapidly with distance, so that some simplification is possible by restricting the summation to nearest neighbour pairs. But even this added simplification does not lead to an exact solution of the problem.

Knowledge that exchange forces are responsible for ferromagnetism, has led to many semiquantitative conclusions of great value. It allows us to rationalize the appearance of ferromagnetism in some metals and not in others.

Assuming that the exchange forces are effective only between nearest neighbours and all the atoms have the same spin S, the exchange energy between one atom and all the surrounding atoms is then.

$$E_{ex} = Z(-2J_{ex}S^2)$$

Where Z is the coordination number of the crystal structure that is each atom have Z nearest neighbours.

$$\text{and} \quad J_{ex} = \frac{3KT_c}{2Z\, S(S + 1)}$$

Where T_c is the curie temperature.

It is usually assumed that exchange forces depend mainly on interatomic distances and not on any geometrical regularity of atom position. Crystallinity is therefore not requirement for ferromagnetism.

There have been two points of view in interpreting spin configurations in ferromagnetic materials. One is based on a localized model in which the electrons

22

responsible for ferromagnetism are regarded as localized at the respective atomic sites. The other point of view is an itinerant or collective electron model in which electrons responsible for ferromagnetism are thought of as wandering through the crystal lattice. .

According to the localized moment theory, the electrons responsible for ferromagnetism are attached to the atoms and can not move about in the crystal. These electrons contribute a certain magnetic moment to each atom and that moment is localized at each atom. This view is implicit in the molecular field theory, either in the original form given by Weiss or in the quantum mechanical form obtained by substituting the Brillouin function for the Langevin. This theory in general explain the variation of the saturation magnetization σ_s with temperature and the Curie–Weiss law, at least approximately, above T_c.

But it can not explain the fact that the observed moment per atom M are nonintegral for metals. Since the moment is entirely due to spin, the magnetic moment per atom due to localized electrons, should be an integer. Other defects of the theory are that M and the molecular field constant w_c are different above and below the Curie temperature.

The collective electron theory emphasize the fact that the electrons responsible for ferromagnetism are considered to belong to the crystal as a whole. Here the electron can move from one atom to another rather than being localized at the positions of the atoms. This theory accounts quite naturally for the nonintegral values of the moment per atom. It also explains fairly well the relative magnitudes

23

of M in iron, cobalt and nickel and the value of the average magnetic moment per atom in certain alloys. These are important accomplishments of the theory. However, the band theory, at least in its simple form, can not account for those alloys which depart from the Slater-Pauling curve.

The general conclusion is that the molecular field theory, with its attendant assumption of localized moments, is not simply valid for metals. Instead, the band theory is regarded as basically correct, and the problem then becomes understanding the precise from of the various bands, how they are occupied by electrons, how the exchange forces operate etc.
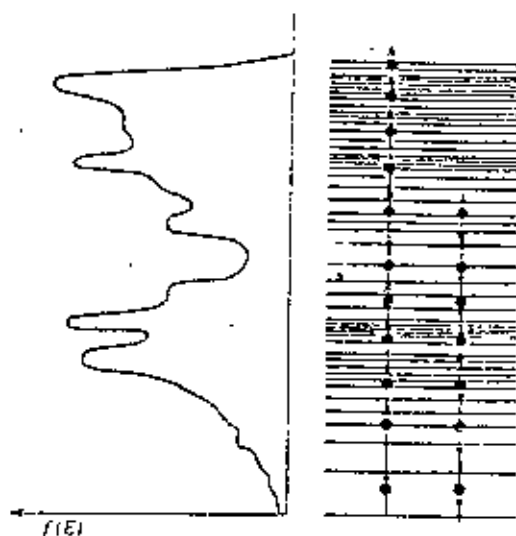
Fig. - 2.5 : State-density curve of 3d band of Nickel and the arrangement of spins in the band

On the basis of the knowledge of the density of states in the 3d shell of copper as calculated by Krutter[9], Slater assumed that the density of states in nickel may be also very high at the top of the 3d band as it is for copper. The density of states in the 3d shell of nickel as a function of energy as calculated by Koster[10] is shown in the figure(2.5). The corresponding energy levels, each of which can be occupied by two electrons, one of plus spin and one of minus spin (Pauli principle) is also shown in this figure (2.5). In order to have a net magnetic moment, therefore, it is necessary that some minus spin electrons be excited to higher energy levels and reverse the sign of their spins from manus to plus. Such as excitation should not require too much energy in the case of the 3d shell because of the high density states.

If therefore, a positive exchange interaction is acting between 3d electrons, the number of plus spins should increase until they fill up half of the 3d shell, leaving vacant levels in the other half. Then the net magnetic moment will be proportional to the number of vacant levels in the 3d shell. In that case, if we add one electron to the atom, this addition should result in a decrease of 1 Bohr magneton per electron because the electron enters into a vacant minus spin level. In this way we can understand the $-45°$ inclination of the right half of the Slater-Pauling curve.

Neutron diffraction experiments have revealed a number of facts about the magnetic structure of metals and alloys. Several neutron experiments on nickel-rich iron-nickel alloys(11-13) have shown that atomic spins responsible for

25

ferromagnetism are localized in each sort of atom 2.6 μ_B for iron and 0.6 μ_B for nickel. These values are nearly constant over a wide range of composition.

The alloys which contain vanadium or chromium show a great deviation from the main Slater-Pauling curve. Those are vanadium or chromium alloys whose mother metals are cobalt, 50 at% Co-Ni and Nickel. A number of branches is drawn from the main Slater-Pauling curve. This shown in the figure(2.4). Such a rapid diminution of the average magnetic moment with composition may be explained either by assuming an antiferromagnetic alignment of the vanadium or chromium moment[16] or by assuming the filling up of 3d vacancies with the outer electrons of vanadium or chromium [17] atoms.

The saturation magnetic moment even at o°K drops off very sharply at an electron concentration of about 26.6 in a face centered cubic region. It was observed for the 30 at% Ni-Fe alloy that the saturation magnetization recovers its large value as soon as the lattice transforms from face-centered cubic to body centered cubic at low temperatures. The rapid decrease of saturation magnetization in this region is due to some antiferromagnetic alignment of atomic moments.

The +45° slope of the left half of the Slater-Pauling curve has been less adroitly treated by the band theory. One possible explanation is that, if the high density or states portion at the top of the 3d band is able to contain 2.5 electrons, the plus spin band remains full until the minus spin band loses 2.5 electrons. Further loss of electrons would deplete the plus spin band because otherwise the

26

Fermi surface of the minus spin band might drop to too low a level. The loss of plus spin electrons then results in a decrease of atomic magnetic moment.

Zener[19] tried to explain this point in terms of antiferromagnetic alignment of two kinds of atomic moments, $+5\mu_B$ and $-1\mu_B$ for iron, on the two substances of the body-centered cubic lattice.

2.3   MAGNETOSTRICTION

2.3.1   Introduction To Magnetostriction

When a ferromagnetic material is placed in a magnetic field, its dimensions change. This phenomenon was discovered as long back as 1842 by Joule, who for the first time found that an iron rod is increased in length when it is magnetized lengthwise. Later on it was found that changes in dimensions occur not only in iron but for all ferromagnetic materials. Magnetostriction is generally defined as this phenomenon   where the dimensions of a ferromagnetic specimen changes during the process of magnetization, but there are a number of effects, which include, joule effect and volume magnetostriction.

The fractional change in length $\dfrac{dl}{l}$ i.e. the strain caused by an applied stress (here the magnetic field H) is written as

$$\lambda = \frac{dl}{l} \tag{1}$$

27

The value of λ measured at magnetic saturation of a material is called the saturation magnetostriction and is represented by λ_s. However the deformation $\dfrac{dl}{l}$ due to magnetostriction is as small as $10^{-5} \sim 10^{-6}$. Such a small deformation can be conveniently measured by means of a strain gauge technique.

The value of the saturation longitudinal magnetostriction λ_s can be positive, negative or even zero. The value of λ depends on the extent of state of magnetization of the material and hence on the strength of magnetic field applied on the samples. The nature of the variation of the magnetostriction λ with magnetic field H is shown in fig (2.7) is well known that the Process of magnetization in ferromagnetic materials occurs by two mechanisms, (i) domain wall motion at low fields and (ii) rotation of magnetization vector at high fields. Magnetostrictive change in length usually occurs in most cases during the rotation of magnetization.

There are two basic kinds of magnetostriction; one is the spontaneous magnetostriction and the other is forced magnetostriction. Spontaneous magnetostriction occurs in each domain with in the specimen due to Weiss molecular field, when a specimen is cooled below the curie point and forced magnetostriction occurs when a specimen is exposed to fields large enough to increase the magnetization of the domain above its spontaneous value. It is evident that both kinds are due to an increase in the degree of spin order. The spontaneous magnetostriction is difficult to observe directly, but it is evidenced by a local maximum at T_c in the variation of the thermal expansion co-efficient with temperature. The field induced magnetostriction in which λ changes from 0

28

to λ_{s} is caused by the conversion of a demagnetized specimen, made up of large number domains spontaneously magnetized in various directions into a saturated, single-domain specimen spontaneously strained (magnetized) in one direction. The modern understanding of the phenomenon owes much to Stoner[], Neel[22], Van Veek[23], Kittel[24], Callen and Callen[29], Lee and Asgar[26]

2.3.2 The Mechanism of Magnetostriction:

Magnetostriction in ferromagnetic material originates from the interaction between the atomic magnetic moments. If the distance between the atomic magnetic moments is r, the bond angle is Φ, as shown in fig. (2.6),then the interaction energy according to Neel[22] can be expressed as,

$$W(r, Cos\Phi) = g(r) + l(r)(Cos^2\Phi - 1/3)$$

$$+ q(r)(Cos^4\Phi - \frac{6}{7} Cos^2\Phi + \frac{3}{35}) + \qquad (2)$$

The first term g(r) is the exchange interaction term, it is independent of the direction of magnetization. Thus the crystal deformation caused by the first term does not contribute to the usual magnetostriction. But it does play an important role in the volume magnetostriction.
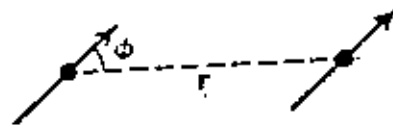
Fig. 2.6 : Interaction between the two magnetic atomic moments

The second term is the dipole dipole interaction which depends on the direction of magnetization and is likely to be the main origin of the magnetostriction. The following higher order terms also contribute to the usual magnetostriction, but normally their contributions are small compared to the dipole-dipole term. Neglecting these higher order terms, the pair energy responsible for magnetostriction can thus be expressed as,

$$W(r, \phi) = I(r) \left(\cos^2\phi - \frac{1}{3}\right) \tag{3}$$

If the direction cosines of domain magnetization is $(a_1\, a_2\, a_3)$ and those of the bond direction is $(\gamma_1,\, \gamma_2,\, \gamma_3)$ the pair energy expression can be written as

$$W = I(r)[a_1\, \gamma_1 + a_2\, \gamma_2 + a_3\, \gamma_3)^2 - \frac{1}{3}] \tag{4}$$

30
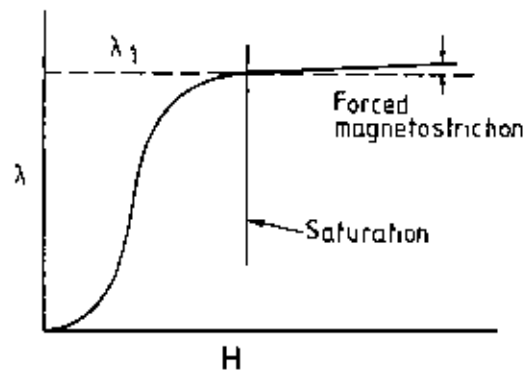
Fig. 2.7: Variation of magnetostriction λ with field H (schematic)

Now consider a deformed simple cubic lattice whose strain tensor components are given by e_{xx}, e_{yy}, e_{zz}, e_{xy}, e_{yz}, e_{zx}. Under the crystal strain each pair changes its bond direction as well as its bond length. For instance, a spin pair with its bond direction parallel to the x axis have the direction cosines $\gamma_1 = 1$, $\gamma_2 = \gamma_3 = 0$; and has an energy in the unstrained state

$$W_x = I(r)(a_1^2 - \frac{1}{3})$$ (5)

Where as, if the crystal strains, its bond length r_0 will be changed to $r_0(1+e_{xx})$ and the direction cosines of the bond direction will be changed to $\gamma_1 = 1$, $\gamma_2 = \frac{1}{2} e_{xy}$, $\gamma_3 = \frac{1}{2} e_{zx}$. Then the pair energy W_x will be changed by the amount,

$$\Delta W_x = (\frac{\delta I}{\delta r}) r_0 e_{xx} (a_1^2 - \frac{1}{3}) + I a_1 a_2 e_{xy} + I a_3 a_1 e_{zx}$$

Similarly, for y and z pairs

$$\Delta W_y = (\frac{\delta I}{\delta r}) r_0 e_{yy} (a_2^2 - \frac{1}{3}) + I a_2 a_3 e_{yz} + I a_1 a_2 e_{xy}$$

$$\Delta W_z = (\frac{\delta I}{\delta r}) r_0 e_{zz} (a_3^2 - \frac{1}{3}) + I a_3 a_1 e_{zx} + I a_2 a_3 e_{yz}$$

Adding these for all nearest neighbour pairs in a unit volume of a simple cubic lattice, we have the magneto-elastic energy

$$E_{mag\,el} = B_1[e_{xx}(a_1^2 - \frac{1}{3}) + e_{yy}(a_2^2 - \frac{1}{3}) + e_{zz}(a_3^2 - \frac{1}{3})]$$

$$+ B_2 (e_{xy}a_1a_2 + e_{yz}a_2a_3 + e_{zx}a_3a_1)$$ (6)

where $B_1 = N(\frac{\delta I}{\delta r})r_0$, $B_2 = 2NI$

32

The energy thus expressed in terms of lattice strain and the direction cosines of domain magnetization is called the magnetoelastic energy.

Magnetoelastic energy of the body-centered cubic lattice have the same expression as equation(6) with

$$B_1 = \frac{8}{3} \, NI, \quad B_2 = \frac{8}{9} \, N[1+(\frac{\delta I}{\delta r})r_o]$$

Similar calculations for the face-centered cubic lattice have the same expression with

$$B_1 = \frac{1}{2} \, N[6I + (\frac{\delta I}{\delta r})r_o] \quad \text{and} \quad B_2 = N[2I + (\frac{\delta I}{\delta r})r_o]$$

Since the magnetoelastic energy (6) has a linear dependence on strain e_{xx}, e_{yy}, e_{zz}, e_{xy}, e_{yz}, e_{zx} the crystal will deform without limit unless it is counterbalanced by the elastic energy which, for a cubic crystal, is given by

$$E_{el} = \tfrac{1}{2}C_{11}(e_{xx}^2 + e_{yy}^2 + e_{zz}^2) + \tfrac{1}{2}c_{44}(e_{xy}^2 + e_{yz}^2 + e_{zx}^2) + C_{12}(e_{yy}e_{zz}+e_{yy}. \, e_{xx} + e_{zz} \, e_{xx})$$

Where C_{11}, C_{44} and C_{12} are the elastic modulie. Since the elastic energy is a quadratic function of the strain of the crystal, it increases rapidly with increasing strain, so that equilibrium is attained at some finite strain.

The condition of equilibrium is to minimize the total energy

$$E = E_{maget} + E_{el} \tag{7}$$

That is $\dfrac{\delta E}{\delta e_{xx}} = B_1(a_1^2 - \dfrac{1}{3}) + C_{11}e_{xx} + C_{12}(e_{yy} + e_{zz}) = 0$

$\dfrac{\delta E}{\delta e_{yy}} = B_1(a_2^2 - \dfrac{1}{3}) + C_{11}e_{yy} + C_{12}(e_{zz} + e_{xx}) = 0$

33

$$\frac{\delta E}{\delta e_{zz}} = B_1(a_3{}^2 - \frac{1}{3}) + C_{11}e_{zz} + C_{12}(e_{xx} + e_{yy}) = 0$$

$$\frac{\delta E}{\delta exy} = B_2 a_1 a_2 + C_{44}\, e_{xy} = 0 \tag{8}$$

$$\frac{\delta E}{\delta e_{yz}} = B_2 a_2 a_3 + c_{44}e_{yz} = 0$$

$$\frac{\delta E}{\delta e_{zx}} = B_2 a_3 a_1 + c_{44}e_{zx} = 0$$

Solving these equations, we have the equilibrium strain

$$e_{xx} = \frac{-B_1}{c_{11} - c_{12}}(a_1{}^2 - \frac{1}{3})$$

$$e_{yy} = \frac{-B_1}{c_{11} - c_{12}}(a_2{}^2 - \frac{1}{3})$$

$$e_{zz} = \frac{-B_1}{c_{11} - c_{12}}(a_3{}^2 - \frac{1}{3}) \tag{9}$$

$$e_{xy} = \frac{-B_2}{c_{44}} \cdot a_1 a_2$$

$$e_{yz} = \frac{-B_2}{c_{44}} a_2 a_3$$

$$e_{zx} = \frac{-B_2}{c_{44}} a_3 a_1$$

The elongation observed in an arbitrary direction of $(\beta_1\ \beta_2\ \beta_3)$ is given by

$$\frac{\delta l}{l} = e_{xx}\ \beta_1{}^2 + e_{yy}\beta_2{}^2 + e_{zz}\beta_3{}^2 + e_{xy}\beta_1\beta_2 + e_{yz}\beta_2\beta_3 + e_{zx}\beta_3\beta_1 \tag{10}$$

If the domain magnetization is along [100] the elongation in the same direction is obtained by putting $\alpha_1 = \beta_1 = 1$, $\alpha_2 = \alpha_3 = \beta_2 = \beta_3 = 0$ in eqn. (10)

thus, $\lambda_{100} = -\dfrac{2}{3} \cdot \dfrac{B_1}{c_{11} - c_{12}}$ (11)

Similarly, when the magnetization is along [111], direction, the

elongation is $\lambda_{111} = -\dfrac{1}{3} \dfrac{B_2}{c_{44}}$ (12)

[By putting $\alpha_i = \beta_i = \dfrac{1}{3}$ in equation (10), where i = 1, 2 and 3]

By using λ_{100} and λ_{111}, equation (10) can be expressed as,

$$\frac{\delta l}{l} = \frac{3}{2} \lambda_{100} (\alpha_1^2\beta_1^2 + \alpha_2^2\beta_2^2 + \alpha_3^2 \beta_3^2 - \frac{1}{3})$$

$$+ 3\lambda_{111}(\alpha_1\alpha_2 \beta_1\beta_2 + \alpha_2\alpha_3\beta_2\beta_3 + \alpha_3\alpha_1\beta_3\beta_1)$$ (13)

This equation is valid for crystals having either [100] or [111] as easy directions. The equation is sometimes written in terms of the constants h_1 and h_2,

where $h_1 = \dfrac{3}{2} \lambda_{100}$ and $h_2 = \dfrac{3}{2} \lambda_{111}$

when the magnetostrictive strain is measured in the same direction as the magnetization, then $\beta_1 = \alpha_1$, $\beta_2 = \alpha_2$, $\beta_3 = \alpha_3$; equation (13) then becomes

$$\lambda_s = \frac{3}{2} \lambda_{100}(\alpha_1^4 + \alpha_2^4 + \alpha_3^4 - \frac{1}{3})$$

$$+ 3\lambda_{111}(\alpha_1^2\alpha_2^2 + \alpha_2^2\alpha_3^2 + \alpha_3^2\alpha_1^2)$$ (14)

Since $(\alpha_1^2 + \alpha_2^2 + \alpha_3^2)^2 = 1 = (\alpha_1^4 + \alpha_2^4 + \alpha_3^4)$

$$+ 2(\alpha_1^2\alpha_2^2 + \alpha_2^2\alpha_3^2 + \alpha_3^2\alpha_1^2)$$ (15)

35

Then the equation (14) may be written as

$$\lambda_s = \lambda_{100} + 3(\lambda_{111} - \lambda_{100})(a_1^2 a_2^2 + a_2^2 a_3^2 + a_3^2 a_1^2) \qquad (16)$$

The generalized expression (13) has greater utility. It allows us (i) to calculate the dimensional change of a single domain due to a rotation of its I_s vector out of the easy direction and (ii) to avoid the uncertainty associated with the demagnetized state in magnetostriction measurements.

The First criteria that a saturated single crystal is a single domain is used to calculate λ_s. Using equation (13) we compute the values of λ_s for two different orientations as I_s in the saturated state, the difference between these two values will yield the strain suffered in a saturated single-domain crystal when I_s rotates from one orientation to the other.

(a)   (b)
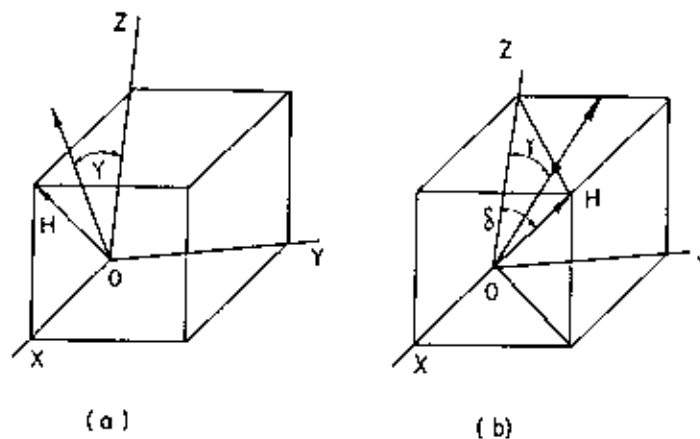
Fig. 2.1: Rotation of magnetization

For example the length of a cube-edge direction [100] in a single domain changes in length as the I_s vector rotates away from it. Let I_s rotate away from [001] direction by an angle δ in the (010) plane. This is shown in the fig. [2.1]. The direction cosines of I_s are $a_1 = \cos(90° - \delta) = \sin\delta$, $a_2 = 0$, $a_3 = \cos\delta$.

36

If the crystal is strained along the [001] direction, therefore, $\delta_1 = \delta_2 = 0$ and $\delta_3 = 1$. Substituting these values into equation (13), we have, saturated magnetostriction in the direction δ,

$$\lambda_s(\delta = \delta) = \frac{3}{2} \lambda_{100}(\cos^2\delta - \frac{1}{3}) \tag{17}$$

When $\delta = 0$, this expression reduces to $\lambda_s(\delta = 0) = \lambda_{100}$

If we take the state of saturation along [001] as the initial state, the strain along [001] direction in a single domain, when I_s rotates by an angle δ away from [001], is

$$\frac{dl}{l} = \lambda_s (\delta = \delta) - \lambda_s (\delta = 0)$$

$$= \frac{3}{2} \lambda_{100}(\cos^2\delta - \frac{1}{3}) - \lambda_{100}$$

$$= -\frac{3}{2} \lambda_{100} \sin^2\delta \tag{18}$$

In iron λ_{100} is positive and [100] is an easy direction. Therefore when I_s rotates through an angle 90° out of an easy direction, the domain contracts fractionally in that direction by an amount

$$= \frac{3}{2} \lambda_{100}$$

The magnetization vector I_s may rotate away from [001] direction in any plane, not only (010) plane and Equation (18) will still apply, because a change in the plane of rotation changes only a_1 and a_2. Much of the original analysis of Magnetostriction has been developed by Akulov[27], Bozorth[26], Hirone[], Chikazumi[2] and Cullity[3] and others.

If the magnetostriction of a particular material is isotropic which is more generally so in the case polycrystalline cubic materials where the crystal axes are randomly oriented throughout the crystal, we can put $\lambda_{100} = \lambda_{111} = \lambda_s$. Then the equation (13) becomes with the introduction of a new symbol,

$$\lambda_p = \frac{3}{2}\lambda_s \left[(\alpha_1^2\beta_1^2 + \alpha_2^2\beta_2^2 + \alpha_3^2\beta_3^2 - \frac{1}{3}) \right.$$

$$\left. + 2(\alpha_1\alpha_2\,\beta_1\beta_2 + \alpha_2\alpha_3\beta_2\beta_3 + \alpha_3\alpha_1\beta_3\beta_1) \right]$$

$$\text{or } \lambda_p = \frac{3}{2}\lambda_s \left[(\alpha_1\beta_1 + \alpha_2\beta_2 + \alpha_3\beta_3)^2 - \frac{1}{3} \right]$$

$$\text{or } \lambda_p = \frac{3}{2}\lambda_s \left(\cos^2\theta - \frac{1}{3} \right)$$

Where λ_p is the saturation magnetostriction at an angle θ to the direction of magnetization, measured from the ideal demagnetized state, θ is the angle between two directions defined by cosines $\alpha_1, \alpha_2, \alpha_3$ and $\beta_1, \beta_2, \beta_3$ then $\cos\theta = \alpha_1\beta_1 + \alpha_2\beta_2 + \alpha_3\beta_3$

CHAPTER 3 PREPARATION OF Fe-Ni ALLOYS & METALLOGRAPHIC STUDY

3.1 PHASE DIAGRAM OF IRON-NICKEL ALLOY SYSTEM

Before the iron-nickel alloys were used as magnetic materials, they were already known to possess certain other peculiar and valuable properties like the low thermal expansion of Invar (36% nickel). This has been known for more than 80 years[1]. Results of investigations of the structure of iron-nickel alloys have been incorporated in the phase diagram of fig (3.1). The alloys important for ferromagnetism lie in the composition range from 40-90% nickel and form a continuous series of solid solutions having a face-centered cubic structure.

The solidification of metal alloys is clearly demonstrated by means of equilibrium diagrams which are convenient graphic representations of changes in state due to variations in temperature and concentrations[3.2]. The equilibrium diagram for a solid-solution alloy system in the fig (3.1) summarizes the essential information obtained from time-temperature curves. In this case, data are plotted for a series of alloys ranging in chemical composition from pure Iron to pure nickel. In fig (3.1) the point A indicates that when the composition is completely free of nickel (pure iron) the liquid phase changes to the solid phase only at the freezing point of Iron. Similarly the data are plotted at the compositions 30% nickel by the points B_1 and B_2. These point fully record the information that the 30% nickel alloy begins to solidify at 1460°C and is completely solid at 1450°C. The data on the chemical compositions of phases are also furnished by this diagram. The complete liquidus and solidus lines are constructed by the use of many pairs of points similar to B_1 and B_2 obtained for other alloy compositions. The liquidus

39
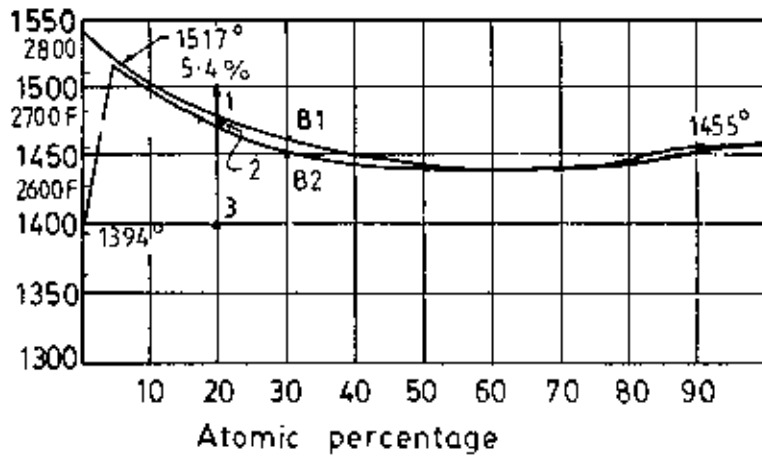
PHASE DIAGRAM

Fig. 3.1: Iron - Nickel alloy system

and solidus lines divide the equilibrium diagram into regions where the liquid phase, liquid and solid phase and solid phase exist.

Since an equilibrium diagram is merely a concise presentation of experimental data obtained on a given alloy system, it follows that the original data can be obtained again from the diagram. The equilibrium diagram is plotted with temperature as the ordinate and composition as the abscissa. Therefore, specific information can be obtained from it only if a temperature and a composition are specified. Such a pair of values locates a point in the diagram. Points of this kind are used repeatedly in analyzing equilibrium diagrams. In our case, the state of the alloy of composition 30% nickel is determined with reference to a certain temperature. Thus, when this alloy is at 1500°C point 1 is determined in fig (3.1) and if this alloy is at 1475°C point 2 is determined. Once the point of interest is located in the diagram, it is easy to ascertain which phase or phases are present. Those phase are present that correspond to the phase field in which the point lies. For example, the 20% Nickel alloy at (1500)°C (point 1) consists of only one phase, the liquid solution. On the other hand, at (1475)°C the same alloy consists of a mixture of liquid solution and solid solution, since point 2 lies in the liquid and solid field of the diagram. At (1400)°C only the solid-solution phase exists. A similar analysis is made for any point (any alloy composition and temperature) in the diagram.

3.2   Preparation of Fe-Ni alloys by powder technology

Fe-Ni alloys of the composition $Fe_{100-x} Ni_x$ (when x = 30, 35, 40, 45, 50 and 78) are prepared from the powders of pure Iron and Nickel of purity 99.9% supplied

41

by B.D.H. England. The required amount of iron and nickel are measured with an accuracy of ± 100μg with a digital balance. The constituent powder of appropriate atomic percent for certain composition are mixed with mortar and pestle in presence of 0.5% of polyvinyl alcohol. Polyvinyl alcohol served as a binder.

The mixture is then pressed into the required form in a die using a pressing machine, "The Metaserv press". The die is first filled with the powder sample and the die plug is placed on top of the powders in the die. The die with the die plug is then placed on the base plate of the pressing machine and a pressure of 6000 psi is applied on the die plug by a hand operated hydraulic jack. After pressing, the hydraulic pressure is released and the die is taken out from the pressing machine. A metal hollow cylinder is placed on the base of the pressing machine and the die with the plug is placed on its top. The outer diameter of the cylinder is the same as that of the die. The cylindrical shaped sample formed is pushed out of the die under pressure. The pressed sample prepared is then sintered.

The sintering process is usually carried out at a temperature below the highest melting points of the constituents. In some cases the temperature used is high enough to form a liquid constituent, such as in the manufacture of cemented carbides, where sintering is done above the melting point of the binder metal. In most cases, the alloy is formed without melting the constituents.

Sintering is essentially a process of bonding solid bodies by atomic forces. Sintering forces tend to decrease with increasing temperature, but obstructions to sintering such as incomplete surface contact, presence of surface films and

42

lack of plasticity etc decrease more rapidly with increasing temperature. Thus elevated temperature tend to favour the sintering process. The longer the time of heating or the higher the temperature, greater will be the bonding between particles and resulting tensile strength.

Despite a great deal of experimental and theoretical work on the fundamental aspects of sintering, there is still much of the process that is not understood. The sintering process starts with bonding among particles as the material heats up. Bonding involves diffusion of atoms where there is intimate contact between adjacent particles leading to the development of grain boundaries. This stage results in a relatively large increase in strength and hardness, even after short exposures to an elevated temperature.

Sintering furnace may be either the electric-resistance type or gas or oil-fired type or induction type. In our case induction type furnace 'P.C.E.' is used. Since bonding between particles is greatly affected by the surface films, the formation of undesirable surface films, such as oxides, must be avoided. This is accomplished by the use of a controlled protective atmosphere.

The pressed sample of the composition $Fe_{70}Ni_{30}$ and $Fe_{65}Ni_{35}$ are sintered at a temperature of 1420°C for 3 hours in the furnace. The furnace is then cooled slowly. The samples of compositions $Fe_{60}Ni_{40}$, $Fe_{55}Ni_{45}$, $Fe_{50}Ni_{50}$ and $Fe_{22}Ni_{78}$ are sintered in the same way at the temperature of 1400°C. For all the samples the duration of sintering is kept three hours and then the furnace is allowed to cool of its own natural rate by switching off the power.

The sintered sample of different compositions of Fe-Ni alloys are annealed at 1000°C in a furnace for 15 hours followed by slow cooling. The magnetic properties of material thus obtained are magnetically more homogeneous and stronger than that of the cast alloys.

X-ray diffractometer investigation are carried out on these samples to check their status and homogeneity. The X-ray diffraction pattern of the samples are shown in Fig. (3.2, 3.3, 3.4). The position of the diffraction peaks are given in table (3.1). It is seen that the diffraction peaks for the samples $Fe_{100-x}Ni_x$ for x = 35 to 78 occurs at identical positions indicating samples maintains identical γ-phase (Fcc), for x = 30, the peaks at 75 and 91 disappears indicating the occurance of phase transformation. This phase can be identified as α-phase (bcc). Thus it appears that x = 30 is the composition at which the phase transition occurs.

3.3   Metallographic Study

Metallography or microscopy consists of the microscopic study of the structural characteristics of a metal or an alloy. The microscope is by far the most important tool of the metallurgist from both the scientific and technical standpoints. It is possible to determine grain size and the size, shape and distribution of various phases and inclusions which have a great effect on the mechanical properties of the metal and also effects the magnetization process through magnetoelastic interaction and the pinning of domain walls of ordered magnetic materials[2,3,5].

The success in microscopic study depends largely upon the care taken in the

preparation of the specimen. The most expensive microscope will not reveal the structure of a specimen that has been poorly prepared. The procedure to be followed in the preparation of a specimen as comparatively simple but involves special care. The steps required to prepare a metallographic specimen properly are as follows:

Sampling : The choice of a sample for microscopic study is very important. If a failure in a metal sample is to be investigated, the sample should be chosen as close as possible to the area of failure and should be compared with one taken from the normal section.

Since our Fe-Ni samples can be considered as mechanically soft, the section is obtained by use of an abrasive cutoff wheel. This wheel is a thick disk of suitable cutting abrasive, rotating at high speed. The friction between the wheel and the sample generates heat. The specimens are therefore, kept cool during the cutting operation by making the wheel pass through water bath in its rotating path.

Rough grinding: The samples are made approximately flat by slowly moving it forward and backword across the surface of the flat smooth file. The specimens are then made rough-ground on a belt spander, with the specimen kept cool by frequent dropping of water during the grinding operation. In all grinding and polishing operations the specimen are moved perpendicular to the existing scratches on its surface. The rough grinding is continued until the surface looks flat and free of nicks, burrs etc and all scratches due to the hacksaw or

45

cutoff wheel are no longer visible.

Mounting : For polishing small size samples, it is required to mount them in some bakelite blocks. Bakelite is used as the most common thermosetting resin for mounting small specimens. Bakelite molding powders are available in a variety of colours, which simplifies the identification of mounted specimens. The specimen and the correct amount of Bakelite powder, or a Bakelite preform are placed in the cylinder of the mounting press. The temperature is gradually raised to 150°C and a molding pressure of about 4,000 Psi was applied simultaneously. Bakelite is set and cured when this temperature is reached. The specimen mount is ejected from the molding die while it is still hot.

Intermediate polishing: After mounting, the specimens are polished on a series of emery papers of successively finer abrasives. The first paper is no. 1, then 1/0, 2/0, 3/0 and finally 4/0 are used.

The intermediate polishing operations using emery paper are done dry. For the next stage of final preparation of the sample, silicon carbide abrasive is used. As compared to emery paper, silicon carbide has a greater removal rate and as it is resin bonded, can be used with a lubricant. Lubricant prevents overheating the samples, minimizes smearing of soft metals and also provides a rinsing action to flush away surface removal products so the paper does not become clogged.

Fine polishing : The final approximation to a flat scratch-free surface is obtained by using a wet rotating wheel covered with a special cloth that is charged with carefully sized abrasive particles. A wide range of abrasives is

available for final polishing. While many will do a satisfactory job, we preferred for the gamma form of aluminum oxide for our iron nickel alloys. The cloth used is silk.

Microstructure of Iron-Nickel Alloys: The iron-nickel alloys contains 30% to as high as 78% nickel. The remainder for these alloys is iron. Micro-structure of the iron-nickel alloys is a simple aggregate of austenite grains. Apart from showing some nonmetallic inclusions, micrographs show only size and shape of the grains, Metallographic examinations are performed on etched specimens.

Etching : The purpose of etching is to make visible the many structural characteristics of the alloys. The process is such that the various parts of the microstructure could be clearly differentiated. This is accomplished by using reagent which subjects the polished surface to chemical action.

Microetching (chemical) : Table-3.2 lists of several etchants that may be used for Iron-nickel or iron-cobalt alloys. As shown in Table 3.3 some of the etchants in Table 3.2 are suitable for both groups of alloys, selection of etchant is often arbitrary. The first etchant listed in Table – 3.2(HCl, $CuCl_2$, $FeCl_3$ HNO_3. methanol and water) is most often used.

Table – 3.1

Angular position (2θ) of the diffraction peaks for
different Fe-Ni alloys.

Composition	2θ position for the peaks						Structure
	1	2	3	4	5	6	
Fe$_{70}$Ni$_{30}$	35	43.6	50.7	56.4	---	----	α-phase (bcc)phase transition
Fe$_{65}$Ni$_{35}$	35	43.5	50.8	---	75	91	γ-phase
Fe$_{60}$Ni$_{40}$	35.5	43.6	50.75	---	75	91	γ-phase (Fcc)
Fe$_{55}$Ni$_{45}$	34.85	43.4	50.6	56	74.6	90.8	γ-phase (Fcc)
Fe$_{50}$Ni$_{50}$	34.8	43.5	50.8	---	74.9	91	γ-phase (Fcc)
Fe$_{22}$Ni$_{78}$	35.4	44.2	51.4	---	75.8	92	γ-phase (Fee)

Table-3.2

Etchants for Microscopic Examination of Iron-Nickel Magnetic Alloys

Etchant	Composition for Chemical Etching	
1	100ml HCl, 2gm $CuCl_2$,7gm $FeCl_3$, 5ml HNO_3, 200ml methanol, 100ml water	Immerse or swab for 10 to 15 sec.
2	15m, HCl, 5gm $FeCl_3$(anhydrous) 60ml ethanol.	Immerse for 5 to 10 sec.
3	3ml HCl, 1ml HNO_3, saturated with $CuCl_2$	Swab for 2 to 3 sec.
4	15ml HCl, 5ml HNO_3, 10ml glycerol	Swab for 10 to 15 sec.
5	Ammonium persulphate (saturated aqueous solution)	Immerse for 20 to 30 sec.
6	2 to 10% nital (HNO_3 in ethanol or methanol)	Immerse for 5 to 10 sec.
7	50ml HCl, 10gm $CuSo_4$, 50ml water (marble's reagent)	Immerse or swab for 5 sec.

Table 3.3

Etchants in table 3 Recommended for Microscopic Examination of Iron-Nickel Alloys

Etchant	Characteristic revealed
1, 2, 4, 5,6	Grain size, structure
3 , 7	Grain size

Intensity

$Fe_{60}Ni_{40}$

$Fe_{65}Ni_{35}$

$Fe_{70}Ni_{30}$

Diffraction Angle 2θ
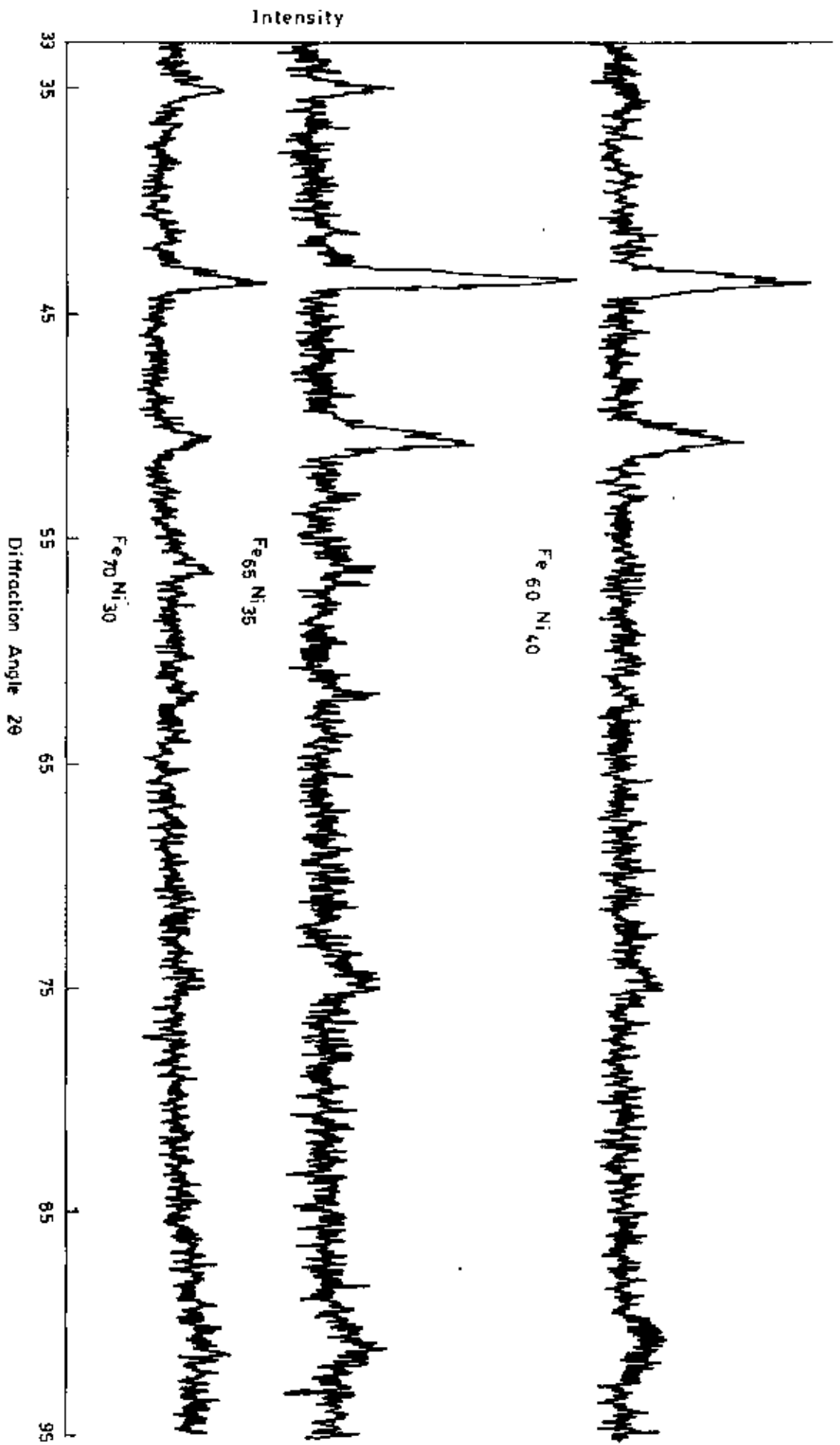
Fig. 3.2

Fig. 3.3

Intensity

Diffraction Angle - 2θ

Fe₅₅ Ni₄₅

Fe₅₀ Ni₅₀

Fig. 3.4

Fe 22 Ni 78
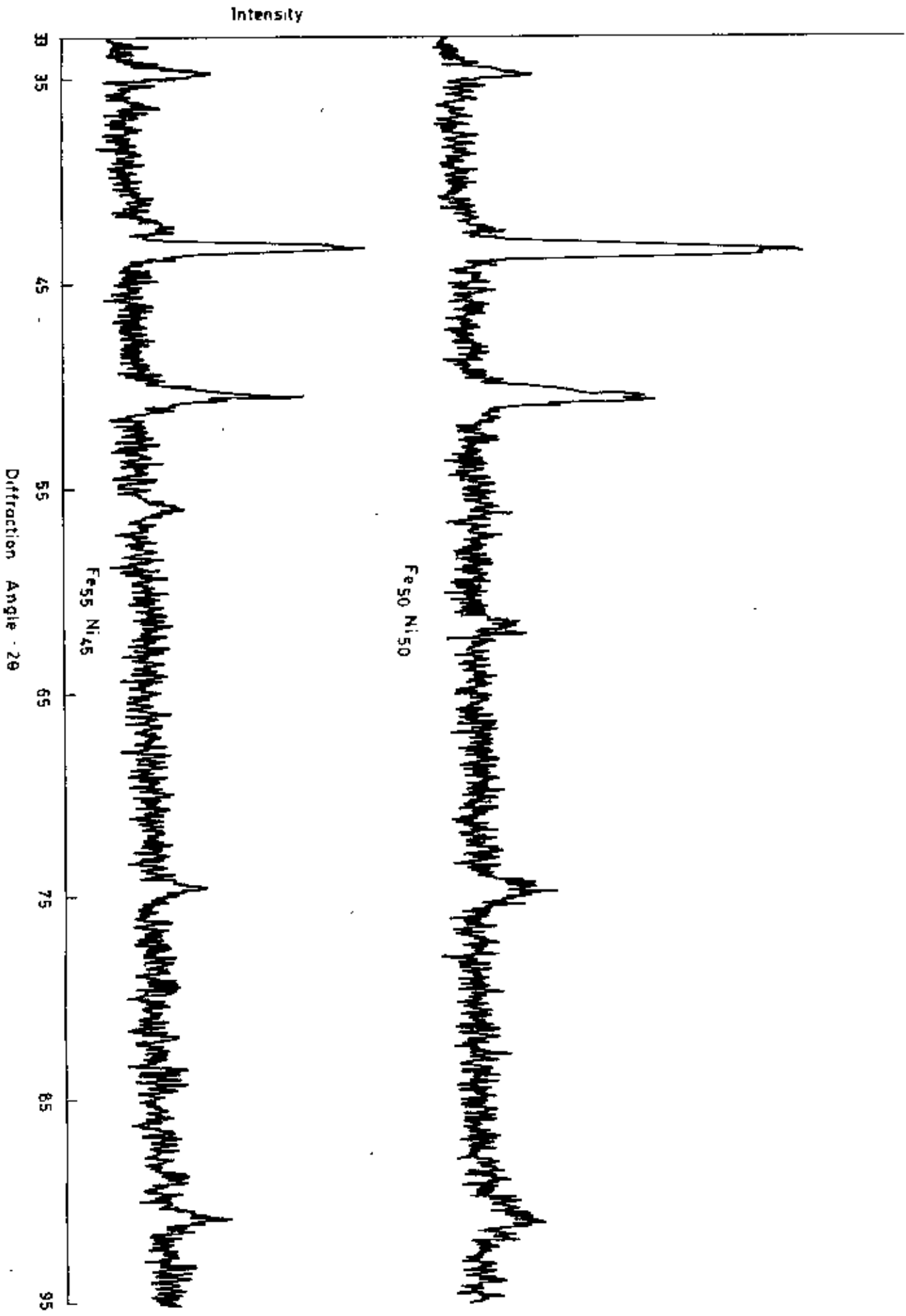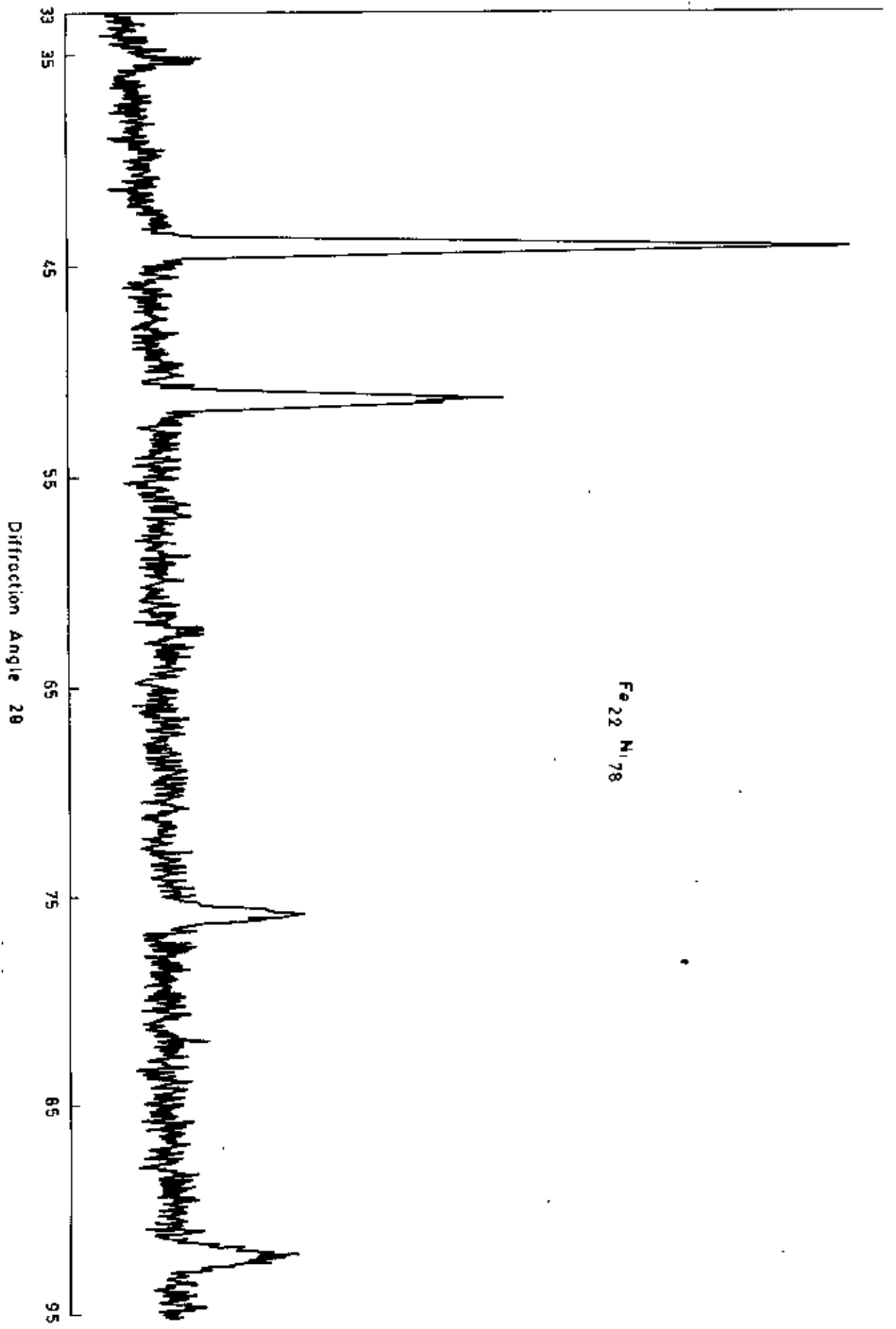
Microstructure of Fe-Ni alloy System

$Fe_{70}Ni_{30}$
with out etching
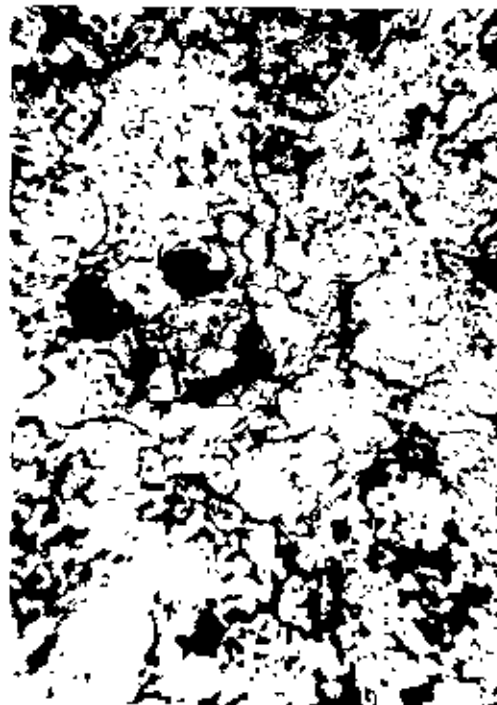
$Fe_{70}Ni_{30}$
with etching
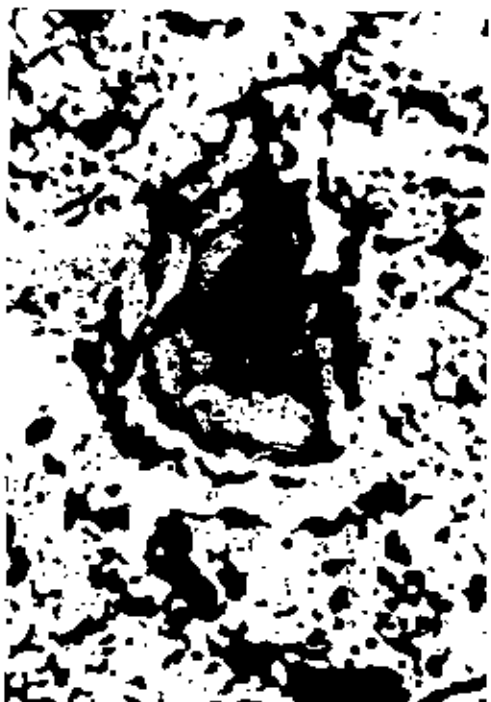
$Fe_{65}Ni_{35}$
with out etching

$Fe_{65}Ni_{35}$
with etching

$Fe_{60}Ni_{40}$
with out etching
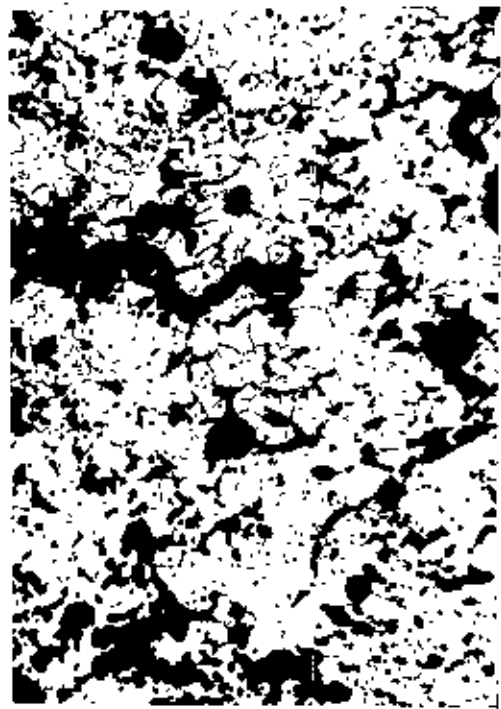
$Fe_{60}Ni_{40}$
with etching
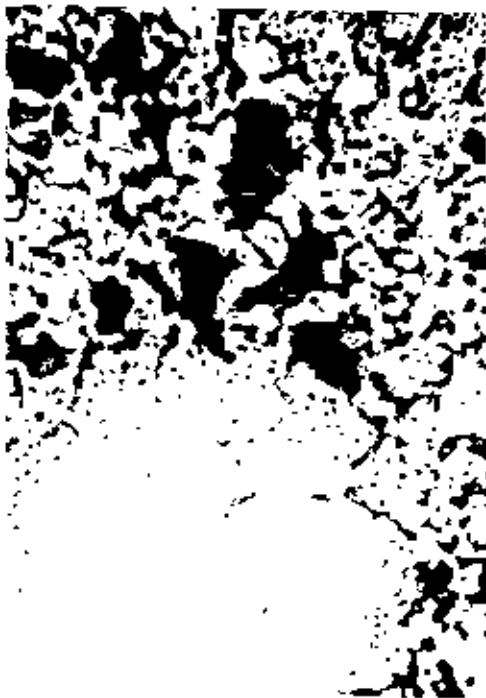
$Fe_{55}Ni_{45}$
with out etching
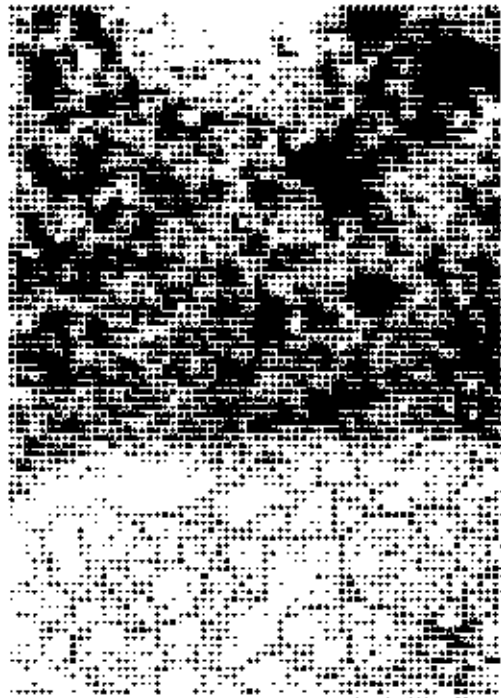
$Fe_{55}Ni_{45}$
with etching

Microstructure of Fe-Ni alloy System

Fe$_{50}$Ni$_{50}$
with out etching
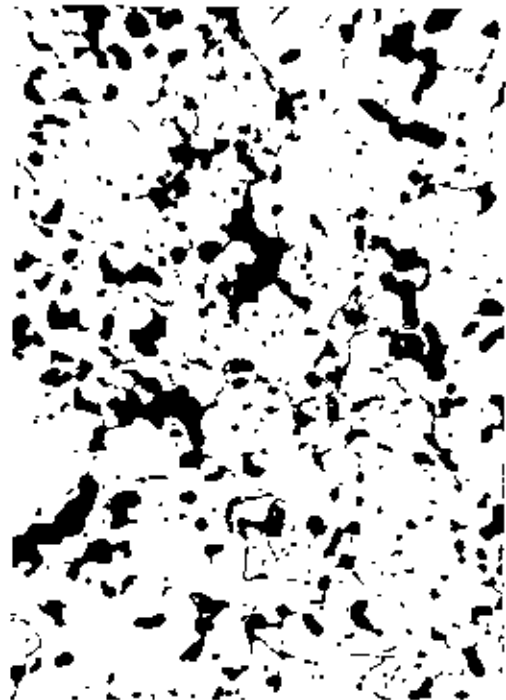
Fe$_{50}$Ni$_{50}$
with etching

Fe$_{77}$Ni$_{77}$
with out etching
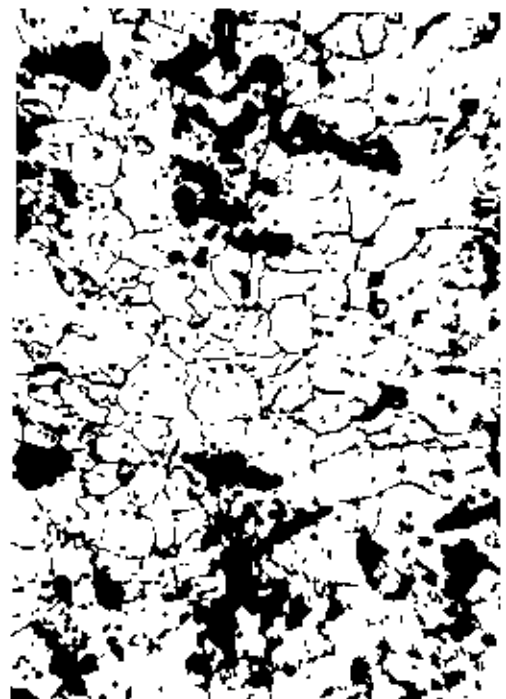
Fe$_{77}$Ni$_{77}$
with etching

CHAPTER 4   MEASUREMENTS OF MAGNETIZATION OF Fe-Ni ALLOY SYSTEM

4.1   DIFFERENT METHODS FOR THE MEASUREMENT OF MAGNETIZATION

There are various methods for the measurement of magnetization based on the following principles.

i.   Measurement of the force acting on the magnetic specimen placed in an inhomogeneous magnetic field.

ii. Measurement of the voltage or current induced by electromagnetic induction.

iii. Measurement of the magnetic field produced by the specimen.

i.   <u>Measurement of the force acting on the magnetic specimen:</u>

When a magnetic specimen is placed in an inhomogeneous magnetic field, the specimen is acted on by a force given by $F_x = M \dfrac{\delta H}{\delta x}$, Where $\dfrac{\delta H}{\delta x}$ is the gradient of the field in the direction x and M is the magnetic moment. Most commonly used method for the measurement of force F_x is the magnetic balance. One arm of the balance suspends the specimen between the pole pieces of an electromagnet while the other arm is balanced by weights or by a current carrying coil placed in a radial magnetic field produced by a small electromagnet.

49

ii.   Measurement of voltage or current induced by electromagnetic induction:

In this method the sample is kept inside a secondary coil. If the magnetic flux inside the secondary coil is changed by changing the magnetization of the specimen (by increasing a magnetic field step wise or by reversing a magnetic field or by removing the specimen from the coil), a voltage $\frac{\delta\phi}{\delta t}$ is induced in the coil. A ballistic galvanometer can be used to detect this induced voltage. The deflection of the galvanometer is proportional to the electric charge which passes through it, which, in this instance, is proportional to the integrated value of $\frac{\delta\phi}{\delta t}$ or to the flux change $\delta\phi$. The proportionality factor can be determined by a standard mutual inductance or by using a standard sample.

iii.   Measurement of the magnetic field produced by the specimen

All the magnetometers are based on this principle. An advanced type of apparatus which belongs to this category is the vibrating sample magnetometer, developed by S. Foner[1-3]. The specimen is vibrated in a vertical direction by a dynamic loudspeaker. In this system a small disc shaped sample is cemented to the end of the specimen rod, the other end of which is fixed to a loudspeaker cone or to some other kind of mechanical vibrator. Current through the loudspeaker vibrates the rod and the sample at about 80 cycles/sec with an amplitude of about 0.1 mm in a direction at right angles to the magnetic field. The oscillating magnetic field of the sample induces an alternating emf in the detection coils. The vibrating rod also carries two reference coils and a reference specimen in the

50
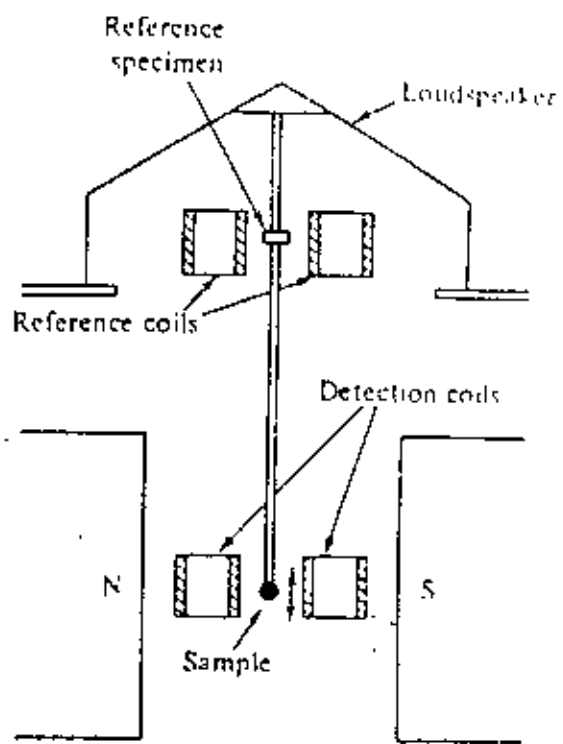
Fig. 4.1 : V.S.M. (Foner type)

form of a small permanent magnet near its upper end. The oscillating field of this sample induces another emf in the two reference coils. The voltages from the two sets of coils are compared and the difference is proportional to the magnetic moment of the sample. This procedure makes the measurement insensitive to changes in, for example vibration amplitude and frequency.

4.2   WORKING PROCEDURE OF THE V.S.M.

In the present measurements the vibrating sample magnetometer used is Foner type. The equipment has been designed and built by the magnetism group of the AECD[4]. The components of the VSM (Fig.4.2) and their working procedure is illustrated below:

In vibrating sample magnetometer, the signal generator (SG) feeds a sine wave signal to the audio amplifier. The frequency of the sine wave from the signal generator is set at 80 Hz. The output of the signal generator is also connected to reference channel input of the lock in amplifier LA.

The drive-rod assembly R tightly coupled to the vibrating papercone of the speaker which vibrates in a vertical direction along its length. By changing the gain of the audio amplifier, the amplitude of vibration may be controlled. A cylindrical shape permanent magnet (P) BaO, $6Fe_2O_3$ is fitted to the drive rod assembly and the sample is fitted to the lower end of the drive rod assembly with the help of a sample holder H.

52

SPEAKER

REFERENCE COIL SYSTEM

Permanent magnet

DRIVE ROD ASSEMBLY

PHASE SHIFTER

RATIO TRANSFORMER

AUDIO AMPLIFIER

LOCK-IN AMPLIFIER

SIGNAL GENERATOR

Sample-Coil System

Sample

Sample Holder
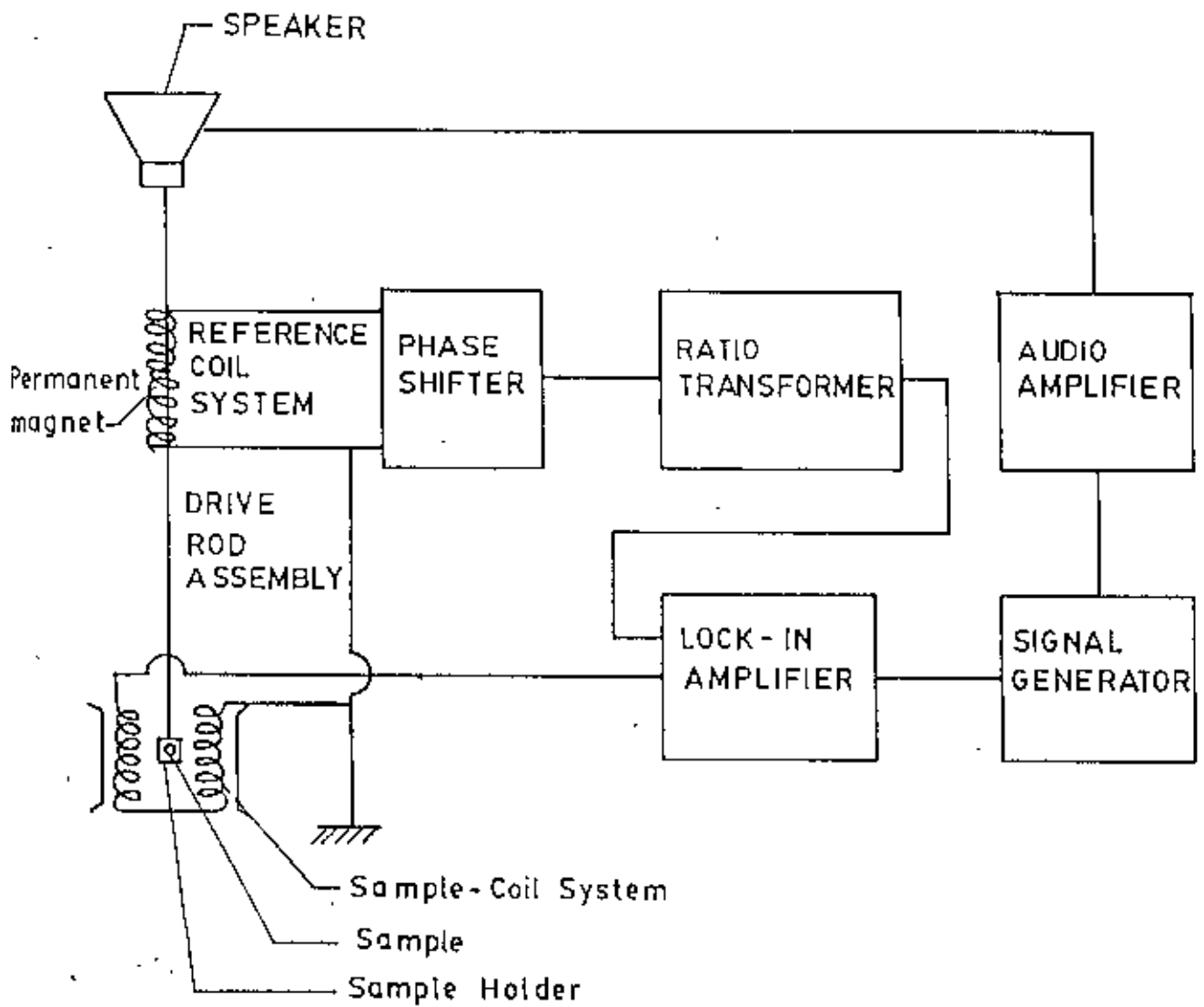
Fig. 4.2 : Block diagram of V.S.M.

53

Two cylindrical sample coils SC are placed symmetrically on either side of the sample and are connected in series opposition to add up the induced e.m.f.'s. The axes of the coils are parallel to the direction of vibration of the sample. This pair of coils is referred to as the sample coil system.

Another pair of coaxial coils RC also connected to each other in series opposition is placed symmetrically around the permanent magnet P. This coil pair is the reference coil system.

As the drive-rod assembly is vibrated with a particular frequency and amplitude, the sample S induces a signal of the same frequency in the sample coil system. This signal is proportional to the dipole moment of the sample. A block diagram of the system used is shown in fig. (4.2).

As the applied magnetic field in the pole-gap is gradually increased by increasing the current through the electromagnet, the sample becomes magnetized more and more and induces a larger signal in the sample coil system till it reaches the state of saturation magnetization. This signal directly goes to one of the inputs of the lock in amplifier. Similarly, another signal of the same frequency is induced in the reference coil system due to vibration of the permanent magnet P. Since the moment of the magnet is fixed, this signal is also of fixed amplitude for a particular frequency and amplitude of vibration. This signal is termed as the reference signal and it is first fed to a unity gain phase shifter unit. The phase shifter is used to bring the reference signal in phase with the sample signal. From the phase shifter the reference signal passes on to the decade ratio transformer R T of constant input impedance. The output

54

of this transformer then goes to the other input of the lock in amplifier. The output to input ratio of the decade transformer can be accurately varied from 10^{-3} to 1. With the help of the decade transformer the amplitude of its output signal is made equal to that of the sample signal. The lock in amplifier is operated in the differential input mode and is used as a null detector.

When the sample signal and the output signal of the decade transformer are of equal amplitude and are in the same phase the D.C. meter of the lock in amplifier gives a null reading.

Since the sample S and the permanent magnet P are vibrated with the same drive rod assembly, the sample signal and the reference signal have a direct phase and amplitude relationship.

4.3   CALIBRATION OF THE V.S.M.

There are usually two methods of calibration of a vibrating sample magnetometer.

i.   By using a standard sample

ii.   By using a coil of small size whose moment can be calculated for d-c current through it.

The VSM used in the present work has been calibrated using a nickel sample of 99.9% purity. The nickel sample is placed in the steady magnetic field in the VSM and the ratio transformer is adjusted until a null is observed in the lock in amplifier. The measurements are done for different field strengths until saturation. The standard saturation moment value of nickel and the ratio transformer reading is used to calculate the calibration constant, K of the VSM following the relation.

$$M = K'K \tag{1}$$

Where M is the magnetic moment, K' is the ratio transformer reading at saturation and K is the calibration constant.

Since $M = m\,\sigma$

$KK' = m\,\sigma$

$$\text{or } K = \frac{m\,\sigma}{K'} \tag{2}$$

Where σ is the specific magnetization and m is the mass of the sample.

The calculated calibration constant is found to be, K =53.474. The accuracy of this calibration depends on the accuracy of the ratio-transformer and the gain of amplifier. The measurement has been done repeatedly for the same standard nickel sample. The calibration constant is estimated to have an accuracy of 1%.

4.4   MAGNETIZATION MEASUREMENTS

The magnetization measurements of Fe-Ni alloys of the composition Fe_{100-x} Ni_x (x = 30,35,40,45,50 and 78) are measured by means of a vibrating sample magnetometer. The magnetization (σ) as a function of magnetic field are measured in different applied fields with a maximum of 5 Kilogauss.

The measurements are confined to room temperature only because of the non-availability of high temperature oven and low temperature cryostat. The magnetization curves are shown in fig. (4.3). It is seen that the magnetization is slowly increasing with the increase of the applied field table (4.1 − 4.6) and curves suggesting that the applied magnetic field of 5 Kilogauss is not sufficient to saturate the specimens. The specific magnetization value σ are then plotted against 1/H, which is found to be linear for higher value of H. The value of σ at $\frac{1}{H}$ = 0 is taken as the value of magnetization at saturation. These curves are shown in fig. (4.4).

The concentration dependence of the saturation magnetization is shown graphically in fig (4.5). The linear increase of the saturation magnetization in iron-nickel alloys with increasing iron concentration is explained in the light of the existing theory as proposed by Friedel[5].

In order to explain the abrupt decrease of the saturation magnetization in iron-nickel alloys around 30 at% of nickel, the localized moment model by Kondorsky and Sedov(1960)[6] and also by Heisenberg are considered.

57

Table - 4.1

Variation of magnetization with magnetic field for sample $Fe_{70}Ni_{30}$.

$$\text{Mass of the sample} = 0.1075 \text{ gm}$$
$$\text{Thickness of the sample} = 1.05 \text{ mm}$$
$$\text{Diameter of the sample} = 4.8 \text{ mm}$$
$$\text{Calibration constant (K)} = 53.474$$

Magnetic field in Kilogauss	Decade Transformer reading K'	Specific magnetization $\sigma_s = \dfrac{KK'}{m} \ Am^2/Kg$
0.1	0.0199	9.8989
0.5	0.0934	46.4602
1.00	0.1428	71.0333
1.5	0.1611	80.1363
1.75	0.1663	82.7230
2.00	0.1703	84.7127
2.25	0.1736	86.3542
2.5	0.1759	87.4983
2.75	0.1779	88.4932
3.00	0.1792	89.1399
3.25	0.1810	90.0352
3.50	0.1820	90.5327
3.75	0.1830	91.0301
4.00	0.1840	91.5275
4.5	0.1855	92.2737
5.00	0.1870	93.0198

Table 4.2

Variation of magnetization with magnetic field for sample $Fe_{65}Ni_{35}$

Mass of the sample = 0.1639 gm

Thickness of the sample = 1.05mm

Diameter of the sample = 5.35mm

Calibration constant K = 53.474

Magnetic field in kilogauss	Decade Transformer reading K'	Specific magnetization $\sigma_s = \dfrac{KK'}{m}$ Am^2/Kg
0.1	0.0429	13.9965
0.5	0.1992	64.9909
1.00	0.2743	89.4930
1.5	0.3006	98.0737
1.75	0.3137	102.3477
2.00	0.3236	105.5777
2.25	0.3312	108.0572
2.5	0.3370	109.9495
2.75	0.3415	111.4177
3.00	0.3450	112.5596
3.25	0.3482	113.6037
3.50	0.3509	114.4846
3.75	0.3530	115.1697
4.00	0.3549	115.7896
4.50	0.3579	116.7684
5.00	0.3605	117.6166

Table 4.3

Variation of magnetization with magnetic field for sample $Fe_{60}Ni_{40}$

Mass of the sample = 0.0655 gm

Thickness of the sample = 0.435 mm

Diameter of the sample = 5.13 mm

Calibration constant K = 53.474

Magnetic field in kilogauss	Decade Transformer reading K'	Specific magnetization $\sigma_S = \dfrac{KK'}{m} Am^2/Kg$
0.1	0.0171	13.9603
0.5	0.0788	64.3320
1.00	0.1096	89.4771
1.5	0.1200	97.9676
1.75	0.1244	101.6597
2.00	0.1270	103.6824
2.25	0.1290	105.3152
2.50	0.1303	106.3765
2.75	0.1317	107.5194
3.00	0.1327	108.3358
3.25	0.1337	109.1522
3.50	0.1343	109.6421
3.75	0.1350	110.2135
4.00	0.1356	110.7034
4.5	0.1364	111.3565
5.00	0.1373	112.0913

Table 4.4

Variation of magnetization with magnetic field for sample $Fe_{55}Ni_{45}$

Mass of the sample = 0.1017 gm

Thickness of the sample = 0.60 mm

Diameter of the sample = 5.50 mm

Calibration constant K = 53.474

Magnetic field in kilogauss	Decade Transformer reading K'	Specific magnetization $\sigma_S = \dfrac{KK'}{m} Am^2/Kg$
0.1	0.0256	13.4605
0.5	0.1127	59.2578
1.00	0.1641	86.2839
1.50	0.1822	95.8007
1.75	0.1874	98.5349
2.00	0.1911	100.4803
2.25	0.1950	102.5312
2.50	0.1974	103.7929
2.75	0.1995	104.8971
3.00	0.2012	105.7909
3.25	0.2030	106.7374
3.50	0.2042	107.3683
3.75	0.2052	107.8941
4.00	0.2061	108.3673
4.50	0.2078	109.2612
5.00	0.2090	109.8924

61

Table 4.5

Variation of magnetization with magnetic field for sample $Fe_{50}Ni_{50}$

Mass of the sample = 0.1600 gm

Thickness of the sample = 1.05 mm

Diameter of the sample = 5.30 mm

Calibration constant K = 53.474

Magnetic field in kilogauss	Decade Transformer reading K'	Specific magnetization $\sigma_s = \dfrac{KK'}{m} \, Am^2/Kg$
0.1	0.0300	10.0263
0.5	0.1675	55.9805
1.00	0.2423	80.9796
1.5	0.2807	93.8134
1.75	0.2981	97.5232
2.00	0.2998	100.1969
2.25	0.3050	101.9348
2.50	0.3092	103.3385
2.75	0.3124	104.4079
3.00	0.3148	105.2100
3.25	0.3170	105.9453
3.50	0.3188	106.5469
3.75	0.3200	106.9480
4.00	0.3214	107.4158
4.50	0.3231	107.9840
5.00	0.3247	108.5187

Table 4.6

Variation of magnetization with magnetic field for sample $Fe_{22}Ni_{78}$

Mass of the sample = 0.1433 gm

Thickness of the sample = 0.95 mm

Diameter of the sample = 5.45 mm

Calibration constant K = 53.474

Magnetic field in kilogauss	Decade Transformer reading K'	Specific magnetization $\sigma_S = \dfrac{KK'}{m}$ Am^2/Kg
0.1	0.0265	9.8887
0.5	0.1188	44.3315
1.00	0.1724	64.3329
1.5	0.1855	69.2214
1.75	0.1882	70.2289
2.00	0.1900	70.9006
2.25	0.1914	71.4230
2.50	0.1926	71.8708
2.75	0.1932	72.0947
3.00	0.1940	72.3932
3.25	0.1944	72.5425
3.50	0.1948	72.6918
3.75	0.1952	72.8410
4.00	0.1956	72.9903
4.50	0.1959	73.1023
5.00	0.1962	73.2142

4.5 RESULTS AND DISCUSSION

The linear increase of the saturation magnetization in iron-nickel alloys with increasing iron concentration is explained by Friedel. Several neutron diffraction experiments on nickel-rich iron-nickel alloys [7-9] have shown that atomic spins responsible for ferromagnetism are fairly well localized in each sort of atom with 2.6 μ_B for iron and 0.6 μ_B for nickel. These values are nearly constant over a wide range of composition. Friedel [5] explained this fact in the following way: When a solute atom with atomic number Z_s is introduced into the metallic matrix composed of the atoms with atomic number Z_n, the excess nuclear charge $(Z_s - Z_n)|e| = \Delta Z|e|$ locally displaces the mobile electrons until the displaced charge exactly screens out the new nuclear charge. In transition metals such a localization of the excess electrons is thought to be particularly perfect because of the high density of states of the 3d shell. For iron-nickel alloys, $Z_s = 26$ for iron and $Z_t = 28$ for nickel; thus $\Delta Z = -2$ and hence the solute iron atom should have two more vacancies in the 3d shell than has a nickel atom in the matrix. It is, therefore, expected that an iron atom in iron-nickel alloys should have two more Bohr magnetos than a nickel atom, which is 2.6 μ_B .

In general, the average magnetic moment of the alloy with concentration C is expressed by,

$$Mav = M_{matrix} - \Delta ZC\mu_B \qquad \qquad \qquad (3)$$

M_{av} represent the average magnetic moment. This is in accord with the right hand half of the slater-Pauling curve and yields a linear increase in magnetization with Iron concentration. The dotted curve is drawn from the calculated values using the relation 3.

64
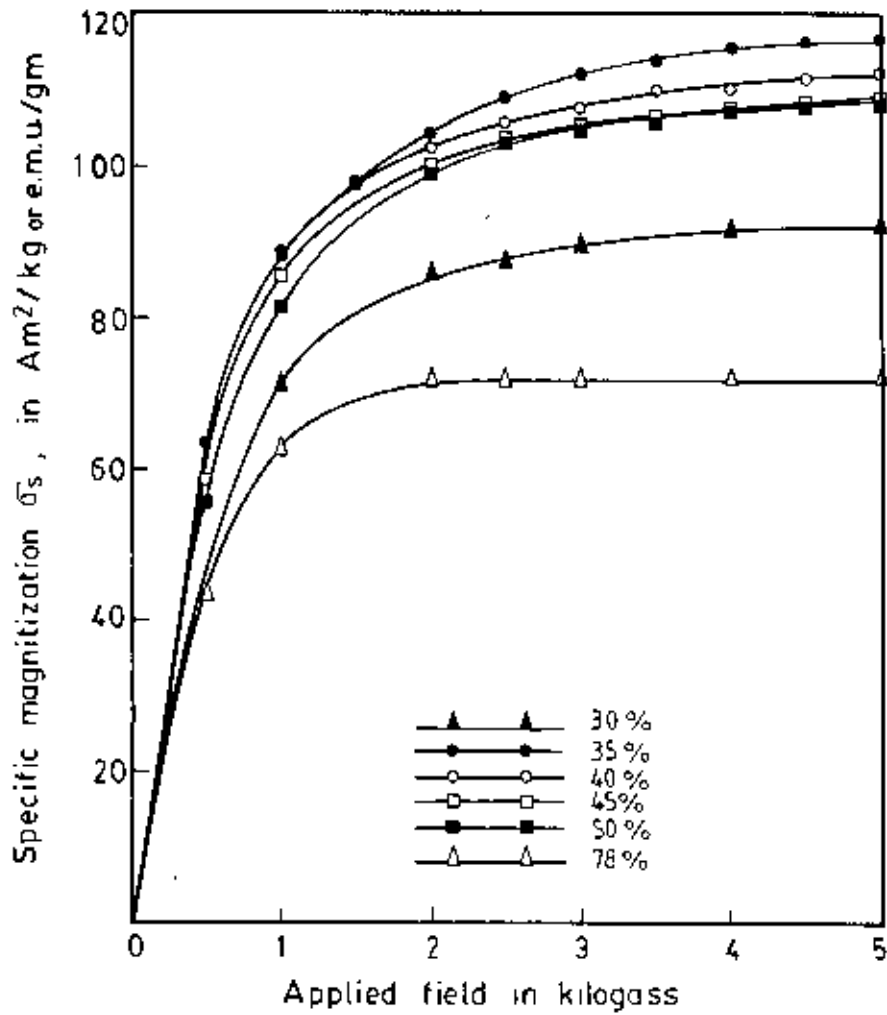
Fig. 4 3   Variation of specific magnetization of $Fe_{100-x}Ni_x$
with applied magnetic field.

65
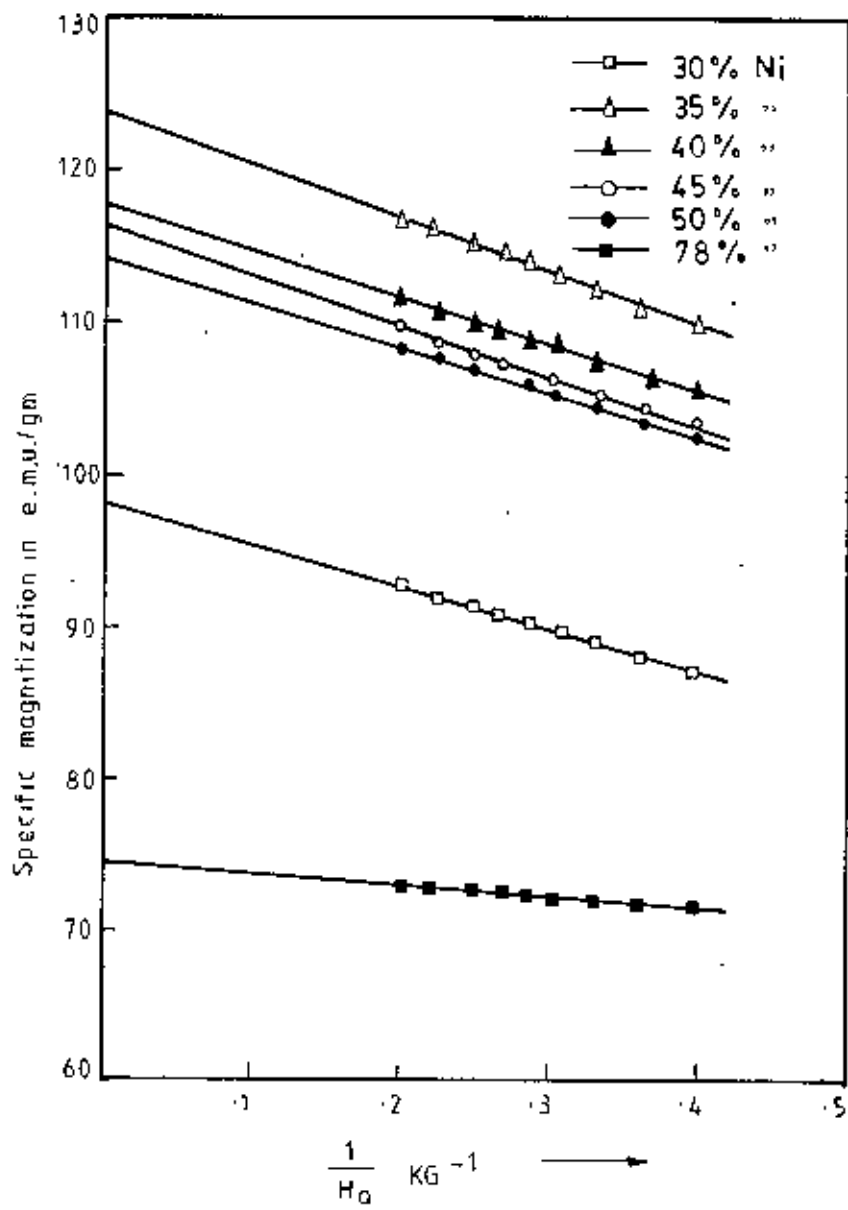
Fig. 4.4: Plot of the specific magnetization of $Fe_{100-x}Ni_x$ against $\frac{1}{Ha}$ [H_a = Applied magnetic field]
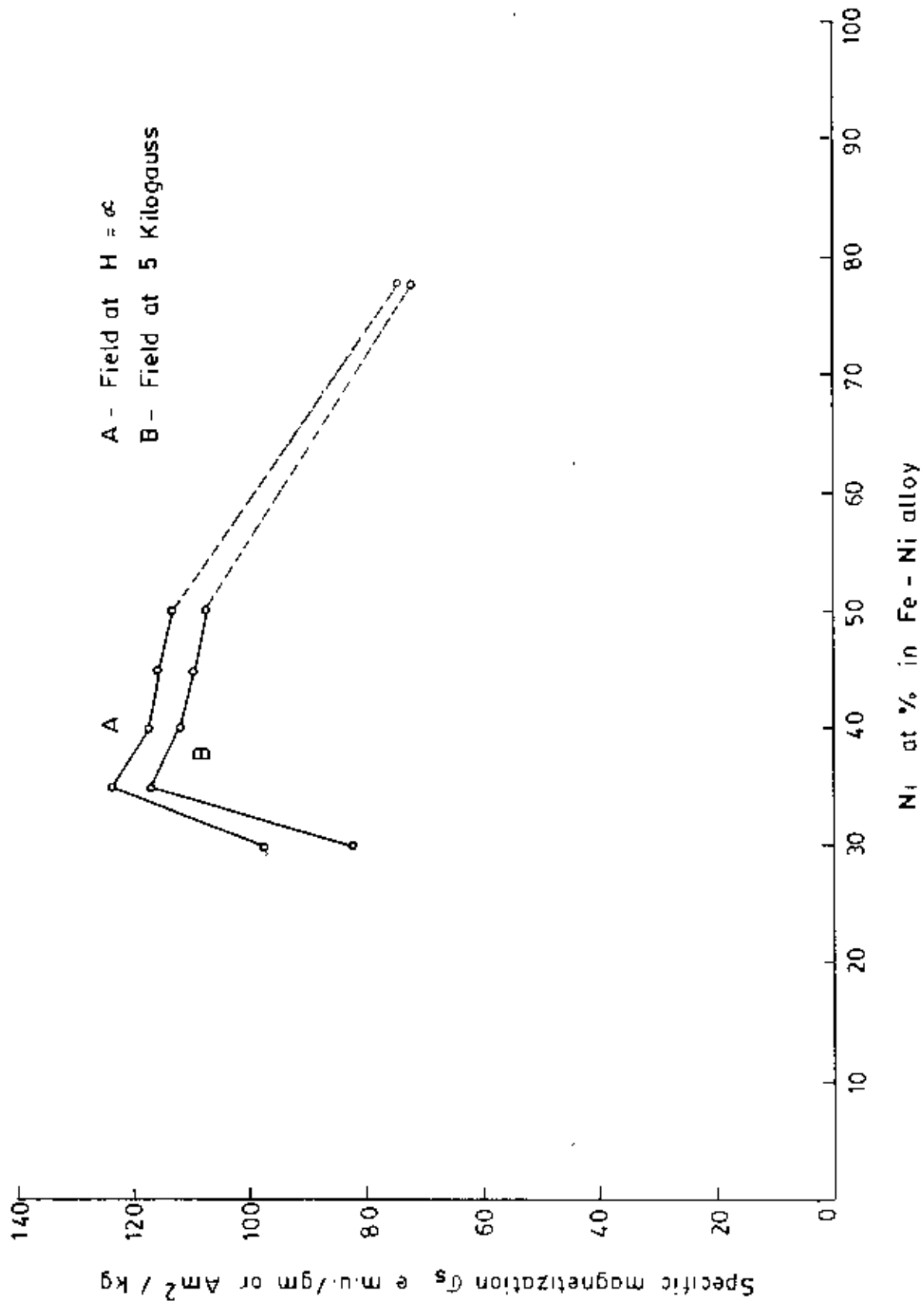
66

Fig. 4.5: The concentration dependence of the saturation magnetization.

A - Field at H = ∝

B - Field at 5 Kilogauss

Specific magnetization σ̄s e.m.u./gm or Am²/kg

Ni at % in Fe - Ni alloy

67

The abrupt decrease of the saturation magnetization in iron-nickel alloys around 30 at% Ni is explained as follows:

For a long time it was thought that the deviation of the average magnetic moment μ_{av} from the Slater-Pauling curve, in Fe-Ni alloys on approach to the γ-α transition is one of the most prominent features of Invar, since it gives obvious indication for the instability of the magnetic moment.

In order to understand the Invar characteristic in 3d-transition metal alloys, there have been two different basic approaches. One is based on the localized electron picture (Heisenberg model)[5] in which each atom has its own permanent and temperature independent moment.

The other is based on the itinerant picture of magnetism (stoner model)[13-14] giving rise to the understanding of the composition dependence of the average moment (Slater-pauling curve).

The first suggestion of the possible presence of antiferromagnetic exchange bonds in 3d-transition metal alloys was proposed by carr [10] that such a mixed exchange situation might explain all deviation from the slater-pauling curve [11-12]. Kondorsky and Sedov later proposed the mechanism described by carr specifically for the case of Fe-Ni Invar and called it latent antiferromagnetism [6,16]. It is generally recognized also by carr [15] that kondorsky and Sedov are the authors of mixed exchange in Invar.

In its simplest form, latent antiferromagnetism has assumed three near neighbour exchange interaction Fe-Fe, Fe-Ni, Ni-Ni [I]. The exchange interaction between Fe-Fe pairs is considered antiferromagnetism. The interaction corresponding to Fe-Ni and Ni-Ni pairs are considered ferromagnetism. The assumed antiferromagnetic bonds are consistent with the known antiferromagnetism of (f.c.c.) γ -Fe[17].

Considering band model [18] one possible explanation is that, if the high density of states at the top of the 3d band is able to contain 2.5 electrons, the plus spin band remains full until the minus spin band loses 2.5 electrons. Further loss of electrons would deplete the plus spin band because otherwise the Fermi surface of the minus spin band might drop to too low a level. The loss of plus spin electrons then results in a decrease of atomic magnetic moment.

CHAPTER 5 MEASUREMENT OF MAGNETOSTRICTION OF Fe-Ni ALLOY SYSTEM

5.1 TECHNIQUE OF MEASUREMENT OF MAGNETOSTRICTION

The change in dimension of a magnetic material in an applied field which we call magnetostriction, is very small of the order of $10^{-5} \sim 10^{-6}$. The measurement of such an small dimensional change can be conveniently measured using an electrical resistance strain gauges. The gauge is cemented to the specimen in a precisely determined direction along which the measurement is required to be made. The use of a strain gauge is based on the assumption that any strain characteristic of the specimen on which the gauges is bonded, is transmitted faithfully to the electrically sensitive zone of the gauge and is observed as a resistance change.

The experimental set up consists of a strain sensing device that is strain gauges, a D.C. bridge, D.C. amplifier and a rotatable electromagnet. A rotatable electromagnet is used to apply the magnetic field in the desired direction. The component elements are arranged in the whetstone bridge fashion.

5.1.1 The Whetstone bridge principle :

The use of Whetstone bridge is quite well known as a convenient method for measuring fractional change in resistance. A D.C. whetstone bridge in slightly out of balance condition is used to measure the fractional change in resistance in the active gauge. The simple type of D.C. bridge circuit is shown in the fig.(5.1).
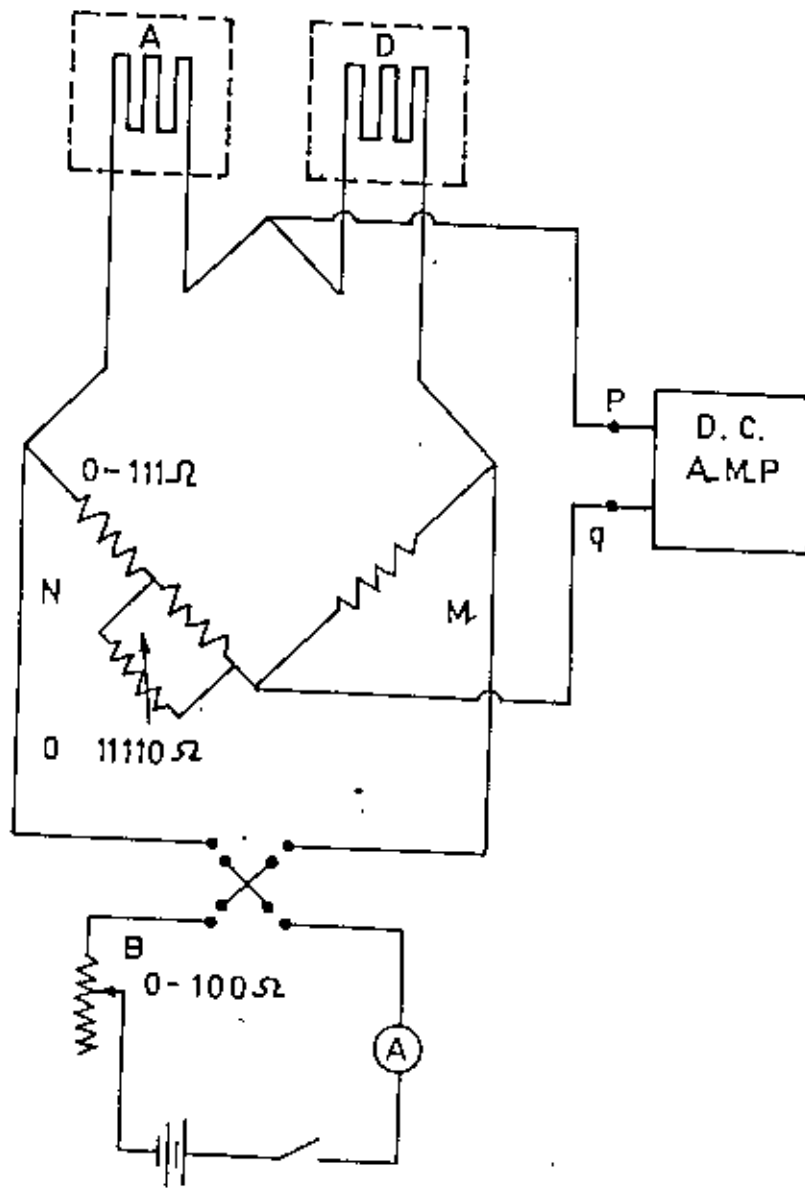
Fig. 5.1   D.C. Wheatstone Bridge circuit

When the resistance of the active gauge is changed from A to A + dA, a corresponding out of balance voltage developes across the input of the D.C. amplifier. Then a deflection is observed in the Nanovoltmeter which is connected to the whetstone bridge circuit.

It the deflection of a Nanovoltmeter is to be used as a measure of the strain, it is necessary to calibrate the Nanovoltmeter. There is a linear relationship between the deflection of the Nanovoltmeter and fractional change in ($\frac{dA}{A}$)resistance under special considerations as discussed below:

5.1.2 Sensitivity and calibration of the D.C. Bridge:

The D.C. bridge used in the present work is similar to that used by Ali Asgar[1]. The current in the D.C. bridge circuit in terms of the Parameters of the bridge is

$$Ig = \frac{E}{(B + D + A + \dfrac{BD}{M})(Z + N + A + \dfrac{ZN}{M})} \times \frac{dA}{(1+K dA)}$$

$$\text{where } K = \frac{M(D + Z) + (B + N)(B + D + Z)}{M(B + D + A + \dfrac{BD}{M})(Z + N + A + \dfrac{ZN}{M})} \quad \cdots \cdots \qquad (1)$$

Equation (1) is an exact algebraic solution for Ig where the circuit on the right hand side of points PQ in fig(5.1) has been treated as a current measuring device of input resistance Z. Since the bridge is only slightly unbalanced K dA<<1 and

72

the factor $1 + K\Delta A$ can be replaced by unity. Also, since the input resistance of the measuring unit is of the order of one megaohm, we can put $Z \to \alpha$ in equation (1) and obtain the expression for the maximum voltage sensitivity corresponding to $B = 0$, close to the balanced condition of the bridge

$$x(\frac{\Delta Ig}{\Delta A})_0 \approx \frac{ED}{(D+A)^2} \qquad \cdots\cdots\cdots\cdots \qquad (2)$$

In our bridge D represents the resistance of the dummy gauge and A that of the active gauge. Both have the same value of 120 ohm in the unstrained condition. Thus the fractional change in resistance can be written as,

$$\frac{\Delta A}{A} = \frac{4Z\Delta Ig}{E} \qquad \cdots\cdots\cdots\cdots\cdots\cdots\cdots \qquad (3)$$

Thus the out of balance voltage $Z\Delta Ig$ measured by the nanovoltmeter maintains a linear relationship with $\frac{\Delta A}{A}$, giving a constant sensitivity. The deviation from linear relationship will only occur if the condition $1+K\Delta A =1$ does not hold. It can be shown that the fractional error involved from this assumption is at most $\frac{\Delta A}{A}$ in our measurements $\frac{\Delta A}{A}$ never exceeded 10^{-3} which corresponds to a fractional error of 0.1%.

The bridge was calibrated by changing the resistance parallel to the 100 ohm resistor in the arm N of the bridge. The minimum strain that can be measured without noise and drift is of the order of 10^{-8} corresponding to 1mm deflection in the nanovoltmeter. The gauge factor of the gauges is 2.09 and the voltage applied to the bridge is two volts. Thus maximum strain sensitivity is 2.5×10^{-6}.

The sensitivity of the bridge can be increased further either by increasing the current in the circuit or by using higher gain in the amplifier. The upper useable limit is determined by the maximum allowable joule heating in the gauges and the signal-to noise ratio.

5.1.3 The choice of Dummy Material

The identical behaviour of the active and dummy gauges is the basic necessity for justifying the use of a compensating gauge for all strain measurements. The nearest approach to this condition can made by subjecting the two gauges to identical strain and thermal conditions. In the present work glass is used as the dummy material for its negligible thermal expansion.

5.1.4 The Specimen Holder

It is very important to keep the thermal environment of the specimen and the dummy identical during the experiment. This is because both the specimen and the dummy are subjected to the heating effect of the gauges and the temperature effect on the active and the compensating gauge should be cancel out in order to find the actual strain in the specimen under investigation. It is necessary either to make the size of the sample and dummy large or to contain them in an enclosure of large heat capacity. The latter method is more convenient. A cylindrical shaped enclosure of copper is used for this purpose and is shown in the fig (5.2). The central portion of the hollow cylinder is Provided with a platform for supporting the dummy and the specimen on its opposite faces. A metallic window is cut which can be closed after mounting the specimen.
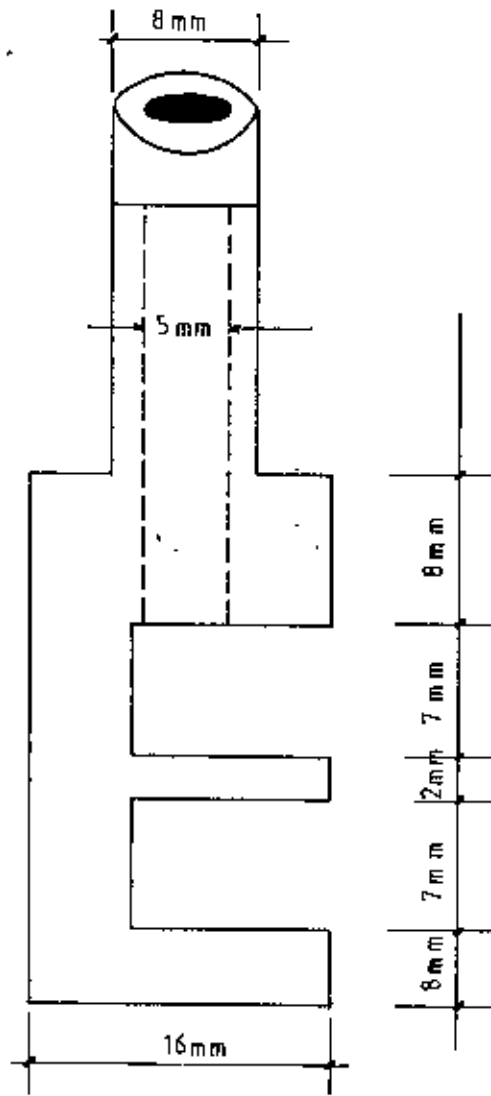
Fig. 5.2: Specimen Holder

The small holes are used to take the electrical leads to the specimen enclosure. The specimen holder is fixed to a specimen rod which is a hollow glass tube. The leads from the active and dummy gauges and also the thermocouple wires pass through the narrow bore of the specimen rod and are connected to the measuring system.

5.1.5 Specimen Mounting

In mounting the specimens in the specimen holder the following factors need to be taken into accounts. The crystal must not be mechanically constrained in the cementing process, otherwise the spontaneous distortions of the crystal that might occur due to temperature change or magnetic field will not be faithfully be transmitted to the strain gauge. When the crystal is elastically soft but highly magnetic, the mechanical constrain may cause the distortion of the symmetry of the crystal. From these points of view the mounting of the specimen should be quite flexible. On the other hand, to avoid any rotation of the specimen due to torque produced by the magnetic anisotropy, the crystal must be held sufficiently rigid with the holder. The best compromise between these two opposing requirements is made by using a thin cork spacer between the specimen and the base of the specimen holder. The specimen is glued to the cork and the cork in turn to the specimen holder. The mosaic pattern of the cork spacer allows the specimen to expand or contract quite freely but constrains it from rotation due to body forces. The arrangement is found to work satisfactorily down to liquid nitrogen temperature.

76

5.1.6 Strain gauge Bonding

The idea of bonding the resistance type strain gauge directly to the material was conceived at California Institute of Technology in the application to a tensor impact test, Rage at Massachusetts. Instituta of Technology at about the same time conceived the idea of bonding the wire to a paper and then bonding the paper with a common glue to the material where the strain is to be measured. This bonded wire type of electrical resistance strain gauge consists of a grid of fine alloy wire bonded to a paper base.

In use this gauga is cemented to the surface of the specimen. It is necessary to have very fine scratches on the gauges and specimen surfaces. The specimen surface is naturally left with fine irregularities of six micron order which is the grain size of the grains of polishing paste used for specimen polishing.

Now some epoxy glue is applied to the gauge surfaces and the gauge area of the specimens. Then the gauge is placed on the specimen surface and the small Pressure is applied for two days on the gauge and the system is allowed to dry at room temperature.

5.1.7 The D.C. Amplifier

To measure the small out of balance D.C. voltage, the model 140 Precision nanovolt D.C. amplifier is used[2]. It acted as a potentiometric amplifier. The voltmeter has a sensitivity of 0.1 microvolt for full-scale deflection, in the highest sensitivity range. The model 140 has selectable gains in decade steps from 100 to 100,000 Gain accuracy is ∓ 100 ppm; gain stability is 50 ppm per

77

three months. A wide dynamic range of input signal levels may be amplified on any gain setting because the model 140 has excellent linearity and low noise.

The model 140 operates either from an A.C. power line when the power supply switch is in the A.C. position, or from its battery in the battery position. For most uses the instrument functions well in A.C. operation mode. Battery operation, may also be used when the A.C. Power line create ground loop or isolation problems. Isolation from low to ground is complete for battery operation when the power cord is disconnected. Also, battery operation is useful to reduce modulation products which may appear at the output during A.C. operation.

5.1.8 Calibration of the Electromagnet

For the production of magnetic field a Varian Electromagnet of pole gap 35mm, is used. The pole pieces of the magnet is of 12.6 cm diameter. The field versus current curve (fig 5.8) for the magnet, is calibrated using Norma Electronic Fluxmeter. Hysteresis effect is observed for increasing and decreasing currents to be negligible. The magnet could be rotated about a vertical axis through the centre of the pole gaps and could be locked in any position. The angular position of the magnet could be read with the help of circular calibraeeted scale fixed at the base graduated in degrees from 0°-360°. The specimen rod along with the specimen holder is hanged from the base of brass plate. The base of the brass plate is put on a heavy wooden platform. The specimen holder along with glass tube is hanged in such a manner that the specimen lies in the homogeneous region of the magnetic field produced by the electromagnet.
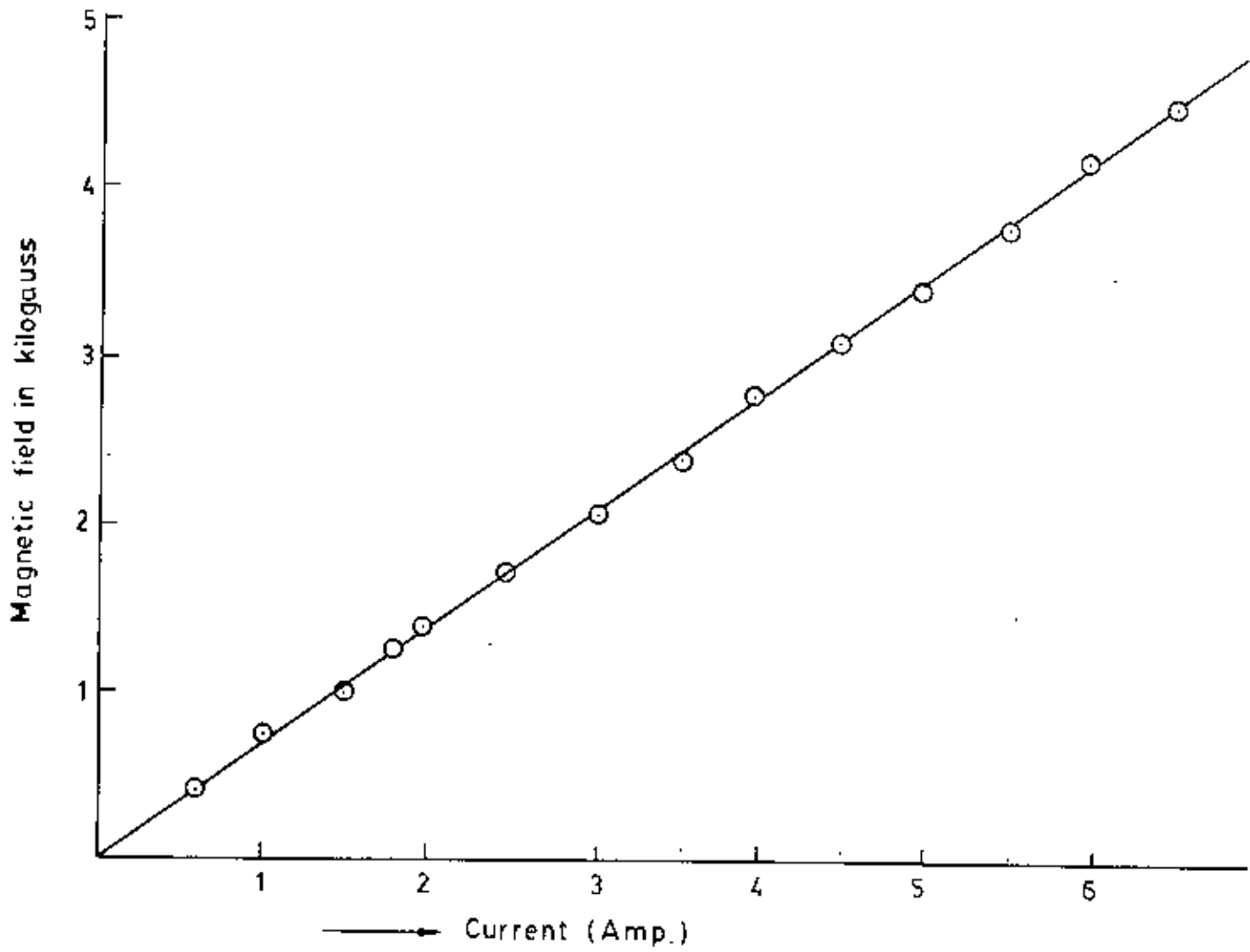
Fig. 5·8   Magnetic field VS Current

79

5.1.9 Strain gauge technique

The strain gauge technique[3] is used in magnetostriction measurement. The gauges can be used on a very small disk shaped specimen cut in a definite crystallographic plane and the gauge can be bonded in a precisely determined direction.

The strain gauge works on the principle that when a fine wire in the form of a grid or a thin foil and embedded in a paper or epoxy film, is bonded firmly on a specimen using a cement or some epoxy glue, it follows the strain of the specimen and shows a change in resistance proportional to the strain.
We can write this relation as

$$\frac{dR}{R} = G \cdot \frac{dl}{l}$$

Where $\frac{dR}{R}$ is the fractional change in resistance, G is the gauge factor and $\frac{dl}{l}$ is the strain along the gauge direction.

The magnetic strain in the crystal is determined from the change in resistance of the gauge fixed on the specimen in relation to the resistance of another dummy gauge bonded on a reference specimen using a resistance bridge in the out of balance condition.

5.2   MAGNETOSTRICTION MEASUREMENT

5.2.1 Bridge Circuit sensitivity and calibration

A d.c. whetstone bridge principle in slightly out of balance condition is used in measuring the fractional change in resistance in the active gauge. A high sensitivity nanovoltmeter of model-140 is used in the circuit. The bridge sensitivity changes linearly with bridge current.

Bridge currents were restricted to a maximum of 25 mA to prevent overheating in the gauge elements. The wheatstone bridge is shown in the figure (5.1). Here A represents the active strain gauge in contact with the specimen and D represents the dummy gauge.

The dummy gauge is in the same environment as the active gauge. Any thermal fluctuations which occured in gauge A, also occured in gauge D and since these are in opposing arms of the bridge, the net effect of the fluctuations should be zero.

By changing the resistance parallel to the 10 ohm resistor in the arm N of the bridge the fractional change in resistance per nanovoltmeter deflection is measured. The fractional change in resistance $\frac{\Delta A}{A}$ per Nanovoltmeter deflection is found to be 2.5×10^{-5}.
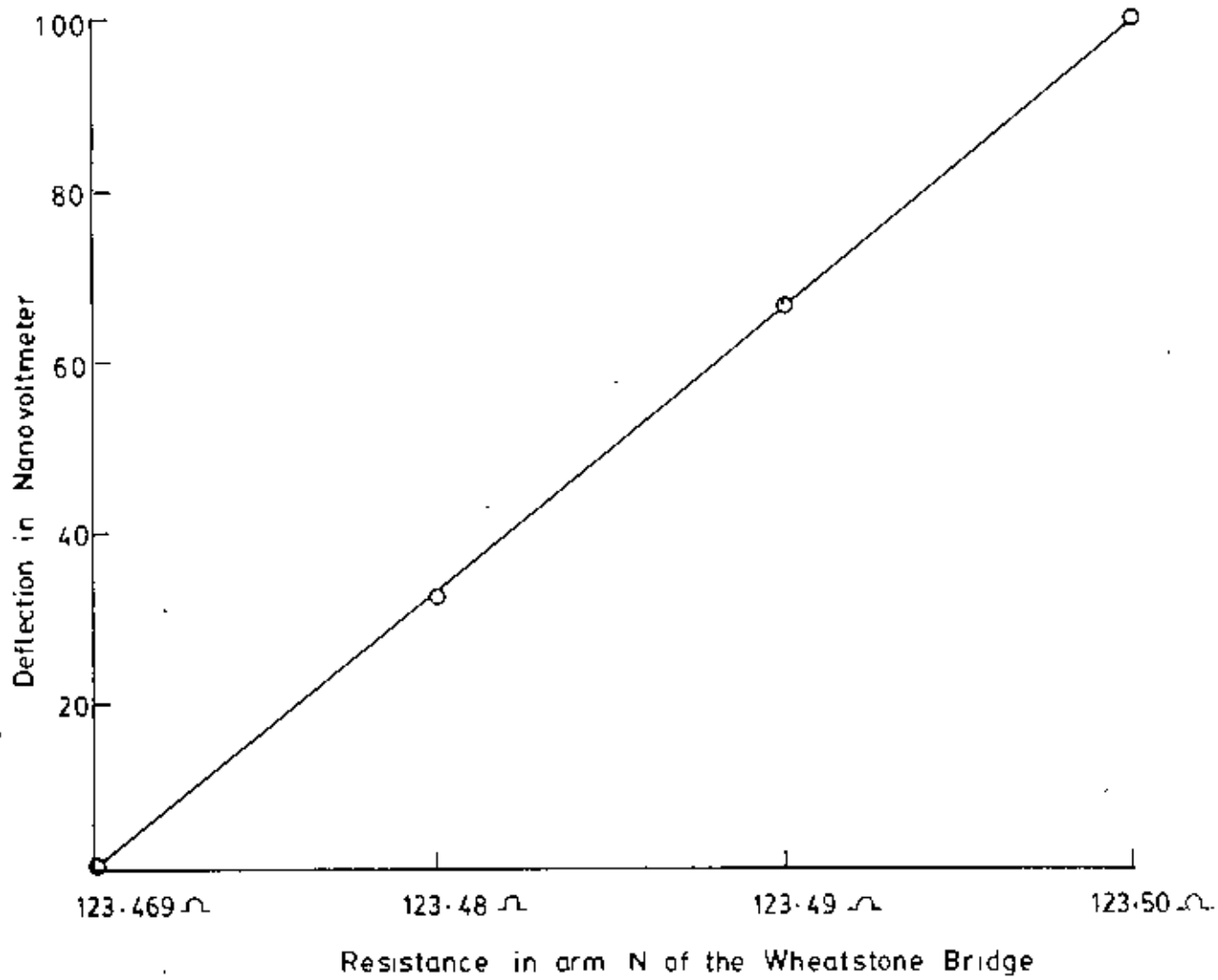
Fig. 5.7 Deflection against change in resistance

5.2.2 Orientation of the gauge position relative to the magnetic field

One feature of ferromagnetic substance is that they exhibit a fairly complex change in magnetization upon the application of the magnetic field. Starting from a demagnetized state (I = H = 0), the magnetization increases with an increase of the field and finally reaches the saturation magnetization which is normally denoted by I_s . Similarly the strain due to magnetostriction changes with increase of magnetic field intensity as shown in fig. (5.5) and finally reaches the saturation value λ. The reason is that the crystal lattice inside each domain is spontaneously deformed in the direction of domain magnetization and its strain axis rotates with a rotation of the domain magnetization, thus resulting in a deformation of the specimen as a whole[4].

When the magnetic field is applied the magnetic domain wall movement starts. In the initial state, if the magnetic field H makes an angle ψ; with the easy axis, the magnetization takes place by the displacement of 180° domain walls until the magnetization reaches the value I_s Cos ψ; during this process no magnetostriction can be observed. The entire magnetization takes place by the displacement of walls, among which only 90° walls are effective in giving rise to the elongation. Thus the magnetostriction depends on the case of displacement of 90° walls relative to that of 180° walls[4]. This gives rise to magnetostriction that is changing lattice dimension. This magnetostriction effect can be looked at as due to predominance of the strain axes in the direction of measurements.

5.3   MEASUREMENT OF MAGNETOSTRICTION

The magnetostriction of Fe-Ni alloys of the composition $Fe_{100-x}Ni_x$ (x = 30, 35, 40 and 78) are measured by means of strain gauge technique as a function of field. The magnetostriction (λ) for different magnetic field is measured with a maximum field of 4 Kilogauss. The measurements are confined to room temperature. The measurements of magnetostriction for the alloy system as a function of magnetic field direction is given in fig. (5.3) and (5.4). These values of the magnetostriction are calculated by using the relation,

$$\lambda = \frac{2}{3G} - \frac{dR}{R}$$

Where sensitivity per nanovoltmeter deflection $\dfrac{dR}{R}$ = 2.5x 10^{-6} and G is the gauge factor.

By determining the difference in deflection in the nanovoltmeter for H along the length of the strain gauge cemented on the specimen and in a direction perpendicular to the length of the strain gauge enables one to calculate λ.

The values of magnetostriction of Fe-Ni alloys of the composition $Fe_{70}Ni_{30}$, $Fe_{65}Ni_{35}$ and $Fe_{60}Ni_{40}$ are listed in table (1), (2) and (3) respectively. And the value of magnetostriction of $Fe_{22}Ni_{78}$ alloy is very close to zero.

Table- 1

Variation of Magnetostriction with magnetic field for Fe_{70} Ni_{30} at room temperature

Gauge factor, $G = 2.09$

$$\text{Sensitivity per deflection } \frac{\Delta R}{R} = 2.5 \times 10^{-6}$$

Field current (Amp)	Magnetic Field strength (Gauss)	Deflection in Nano voltmeter	$\dfrac{\Delta R}{R}$	Magnetostriction λ $= \dfrac{2}{3G}.\dfrac{\Delta R}{R}$
1	750	1.5	3.75×10^{-6}	1.196×10^{-6}
2	1400	3	7.5×10^{-6}	2.3×10^{-6}
3	2100	5	12.5×10^{-6}	3.987×10^{-6}
4	2800	6	15×10^{-6}	4.784×10^{-6}
5	3500	6	15×10^{-6}	4.784×10^{-6}

Table − 2

Variation of Magnetostriction with magnetic field for Fe_{65} Ni_{35} at room temperature

Gauge factor, G = 2.09

Sensitivity per deflection $\dfrac{\Delta R}{R} = 2.5 \times 10^{-6}$

Field current (Amp)	Magnetic Field strength (Gauss)	Deflection in Nano voltmeter	$\dfrac{\Delta R}{R}$	Magnetostriction λ $= \dfrac{2}{3G} \cdot \dfrac{\Delta R}{R}$
0.4	300	4	10×10^{-6}	3.18×10^{-6}
0.6	450	7	17.5×10^{-6}	5.58×10^{-6}
0.8	600	9	22.5×10^{-6}	7.177×10^{-6}
1.0	750	10	25×10^{-6}	7.974×10^{-6}
1.2	875	12	30×10^{-6}	9.569×10^{-6}
1.4	1000	13	32.5×10^{-6}	10.366×10^{-6}
1.6	1125	14	35×10^{-6}	11.164×10^{-6}
1.8	1250	15	37.5×10^{-6}	11.961×10^{-6}
2.0	1400	16	40×10^{-6}	12.759×10^{-6}
2.5	1750	18	45×10^{-6}	14.354×10^{-6}
3.0	2100	19	47.5×10^{-6}	15.151×10^{-6}
3.5	2450	20	50×10^{-6}	15.948×10^{-6}
4.0	2800	20	50×10^{-6}	15.948×10^{-6}

Table — 3

Variation of Magnetostriction with magnetic field for Fe_{60} Ni_{40} at room temperature

Gauge factor, G = 2.09

$$\text{Sensitivity per deflection } \frac{\Delta R}{R} = 2.5 \times 10^{-6}$$

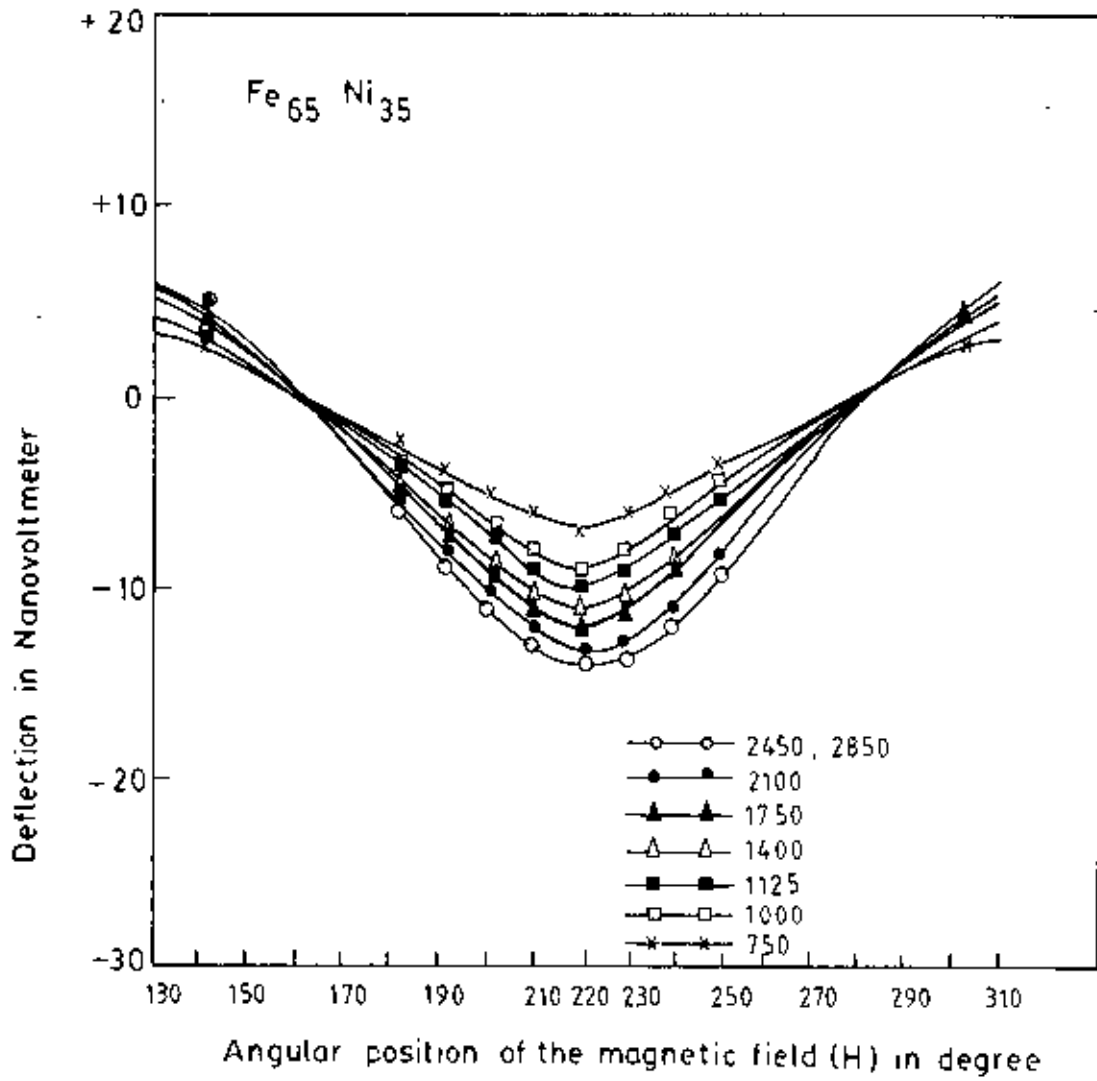| Field current (Amp)	Magnetic Field strength (Gauss)	Deflection in Nano voltmeter	$\dfrac{\Delta R}{R}$	Magnetostriction $\lambda = \dfrac{2}{3G} \cdot \dfrac{\Delta R}{R}$
0.2		3	7.5×10^{-6}	2.39×10^{-6}
0.4	300	6	15×10^{-6}	4.78×10^{-6}
0.6	450	9 ·	22.5×10^{-6}	7.17×10^{-6}
0.8	600	12	30×10^{-6}	9.56×10^{-6}
1.0	750	14	35×10^{-6}	11.164×10^{-6}
1.2	875	16	40×10^{-6}	12.76×10^{-6}
1.4	1000	18	45×10^{-6}	14.35×10^{-6}
1.6	1125	20	50×10^{-6}	15.95×10^{-6}
1.8	1250	22	55×10^{-6}	17.543×10^{-6}
2.0	1400	24	60×10^{-6}	19.14×10^{-6}
2.5	1750	26	65×10^{-6}	20.733×10^{-6}
3.0	2100	28	70×10^{-6}	22.328×10^{-6}
3.5	2450	28	70×10^{-6}	22.328×10^{-6}
4.0	2800	28 ·	70×10^{-6}	22.328×10^{-6}

Fig. 5.3 Variation of the magnetostriction (proportional to the deflection in Nanovoltmeter) against the direction of the applied magnetic field.
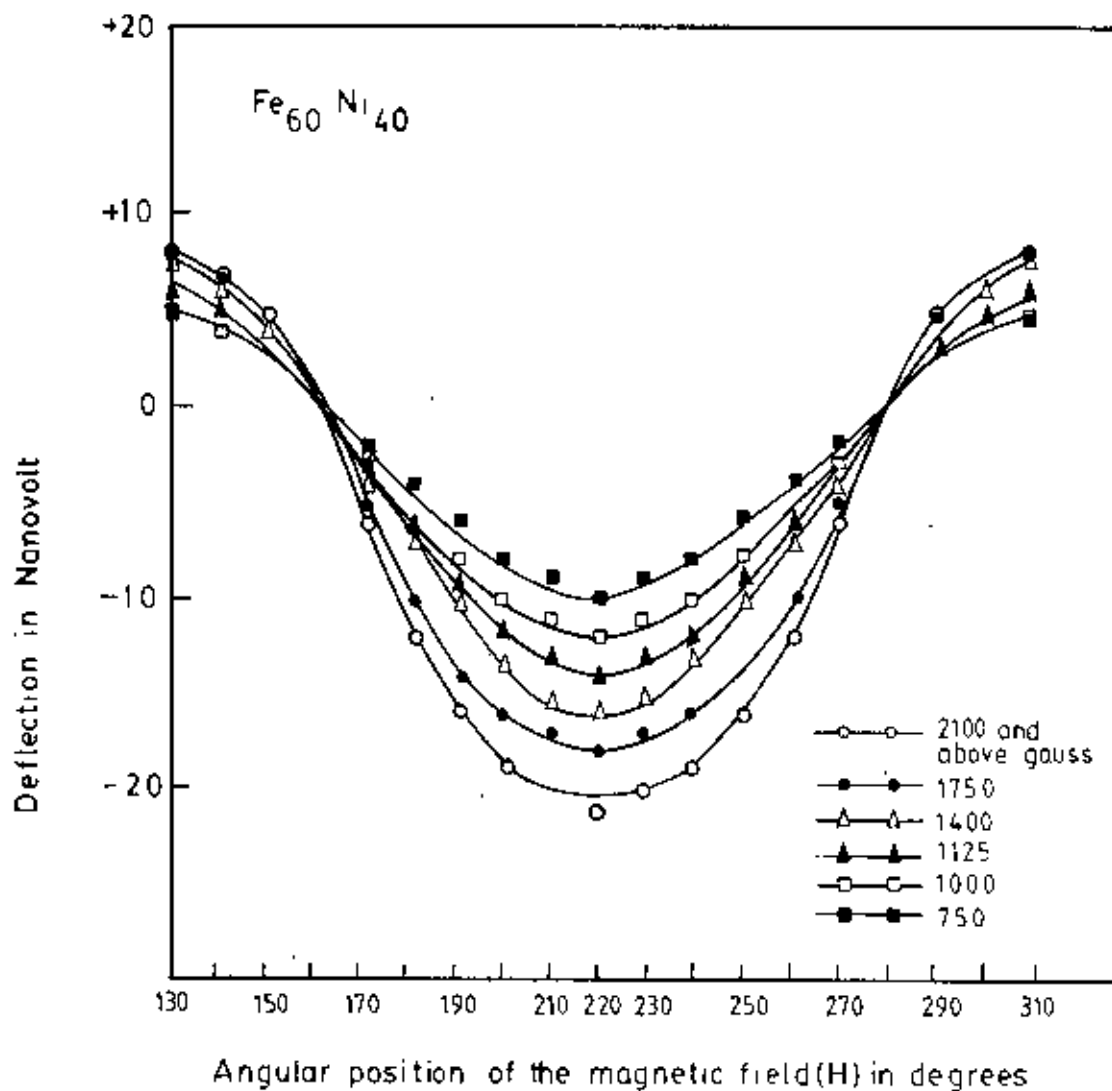
Fig. 5.4: Variation of the magnetostriction (proportional to the deflection in Nanovoltmeter) against the direction of the applied magnetic field.

5.4 RESULTS AND DISCUSSION

The magnetic or quasi magnetic forces between atoms give rise to an expansion or contraction of the lattice by opposing the purely elastic force between atoms. The equilibrium distortion or magnetostriction occurs when the sum of the two corresponding energies is a minimum. The linear magnetostriction is calculated assuming that the magnetic forces between atoms can be simulated by magnetic dipole moments alone.

The values of magnetostriction thus calculate for different specimens are presented in fig. (5.5) as a function of applied field. The curves show that the value of the saturation magnetostriction is lowest for $Fe_{70} Ni_{30}$ specimen and increases with nickel concentration. On the other hand the magnetic field at which the magnetostriction gets saturated is highest for $Fe_{75}Ni_{30}$ alloy (at H = 2800 gauss) and is less for $Fe_{65}Ni_{35}$ (at H = 2450 gauss) and least for $Fe_{60}Ni_{40}$(at H = 2100 gauss).

The higher field needed to saturate the magnetization in alloys with higher concentration of iron indicates that the domain wall movement in this case with the application of the magnetic field becomes more difficult because of the lower value of magnetization, the magnetic force acting on a domain wall being proportional to the product of the magnetization and the applied magnetic field.

Since iron has positive magnetostriction and the magnetostriction of nickel is negative, it is expected by the thumb rule that in an alloy of this two elements magnetostrictive contributions from this elements will tend to cancell each ,the

Magnetostriction, λ

30 × 10⁻⁶
25 × 10⁻⁶
20 × 10⁻⁶
15 × 10⁻⁶
10 × 10⁻⁶
5 × 10⁻⁶

□—□ 30 % Ni
○—○ 35 % ,,
●—● 40 % ,,

500   100   1500   2000   2500   3000   3500
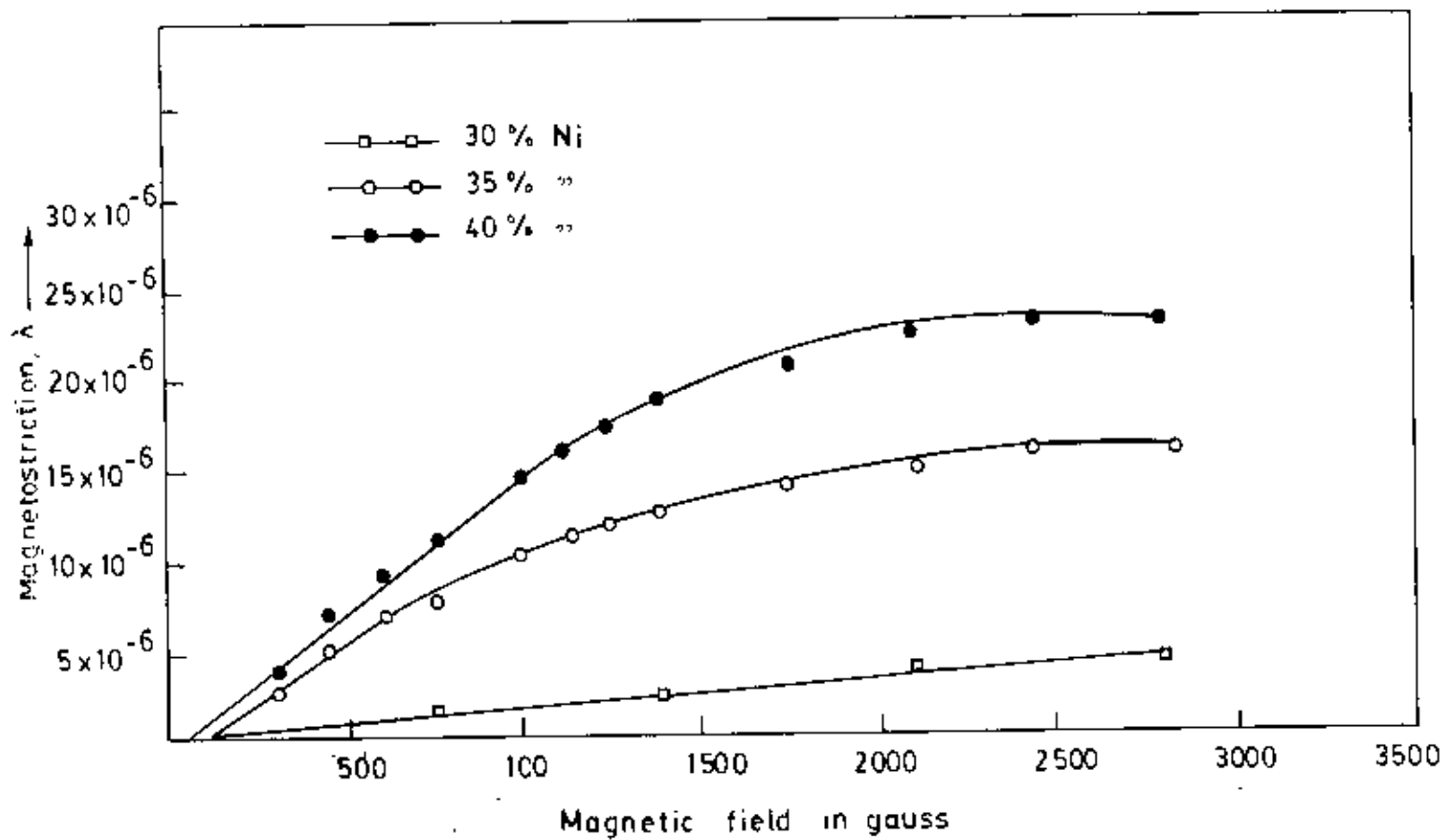
Magnetic field in gauss

Fig. 5.5: Variation of the magnetostriction with applied magnetic field.
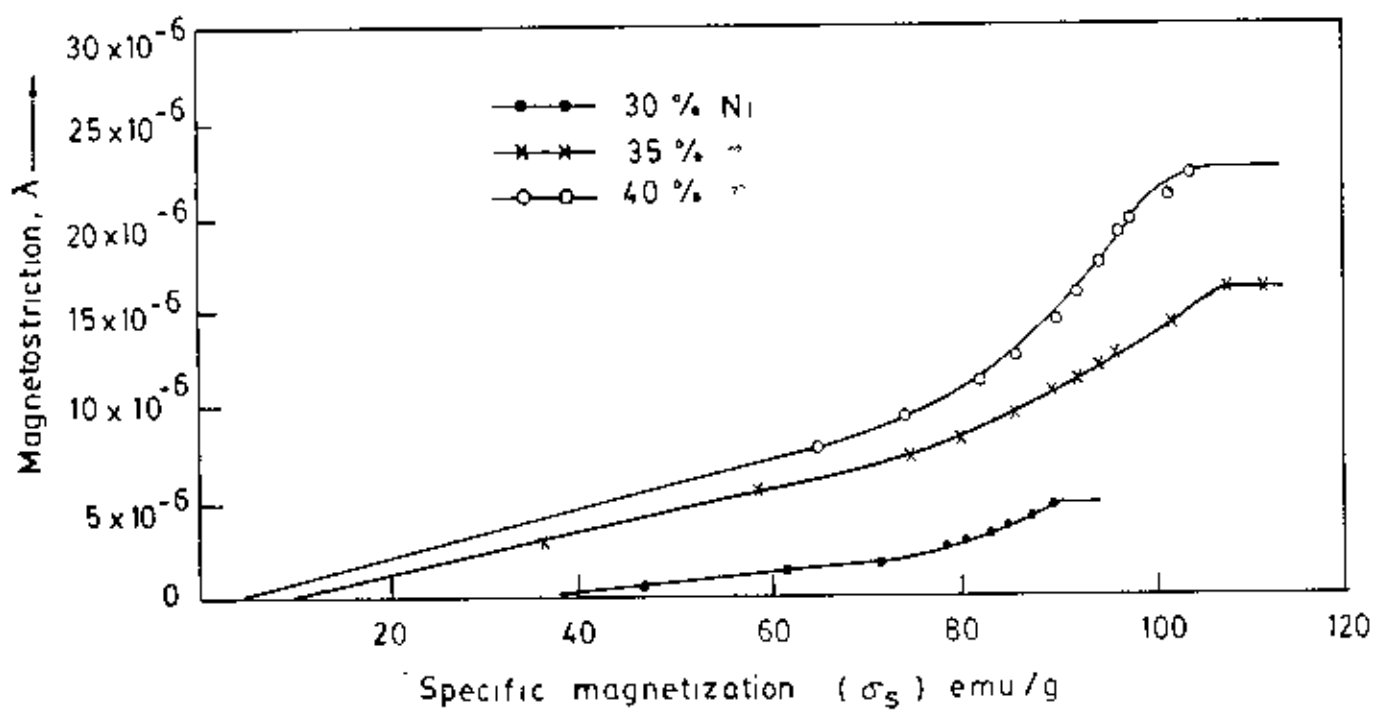
91

Fig.5.6: Magnetostriction as a function of specific magnetization

other. This occurs in our measurements at around 78 at% of nickel. However actual mechanism of magnetostriction being a complex phenomenon of spin orbit interaction, crystal anisotropy and elastic constant, the magnetostriction of the alloy is not likely to show any linearity in respect of the contributions from the constituent elements.

Magnetostriction as a function of specific magnetization of Fe-Ni alloys are plotted in fig. (5.6). This result is interpreted as follows. The $180°$ domain wall movements do not contribute to magnetostriction because the strain axes remains unaltered in this case. The $90°$ domain wall movements on the other hand give rise to magnetostriction. Magnetostriction against Magnetization thus provides important information about the domain wall movements during the magnetization process. As seen from the graph there is very little increase in the magnetostriction with magnetization in the initial part of the graph(5.6). This means initially the magnetization proceeds mostly by the $180°$ domain wall movements. Magnetostriction increases as we proceed towards the saturation in magnetization. This means that the final process of magnetization is mostly due to $90°$ domain wall movement. Some change in magnetization occurs around this point with out any corresponding change in magnetostriction. This, however, can not be resolved completely; because the $90°$ domain wall movement and $180°$ domain wall movement can happen simultaneously. Since magnetostriction reach saturation just before the saturation magnetization is reached, it can only be said that $180°$ domain wall movement continues up to the saturation magnetization point.

From the curve (5.6), it appears that for $Fe_{70}NI_{30}$ alloy, the magnetostriction increases linearly with the specific magnetization until the material attains the

93

magnetization value of 71 e.m.u./gm which is nearly 70% of its saturation magnetization value. For $Fe_{65}Ni_{35}$ and $Fe_{60}Ni_{40}$ alloys the magnetostriction maintains linearity with specific magnetization only up to the state where the materials attains 50% of the saturation magnetization of 124 e.m.u./gm and 118 e.m.u./gm respectively. Beyond which the magnetostriction for all the samples show a nonlinear behaviour untill the magnetostriction get saturated. It is observed that magnetostriction attains its maximum value before the material attains the state of saturation magnetization. For $Fe_{22}Ni_{78}$ alloy, the material did not show any magnetostriction up to the maximum applied magneticfield 3500 gauss.

The saturation magnetostriction of Fe-Ni alloys at the composition 40 at% of Nickel approaches towords maximum. Bozorth[5] associated this with the maximum in the saturation magnetization range of γ-phase alloys[5] which is not the case as appears from our result which gives maximum magnetostriction at 35% Ni. But the magnetostriction of $Fe_{65}Ni_{35}$ Invar show anomalies associated with antiferromagnetic γ-Fe clustering in the ferromagnetic matrix[6].

On approching the $\alpha \rightleftharpoons \gamma$ phase transition boundary the magnetostriction of $Fe_{70}Ni_{30}$ alloy becomes very small. The minimum magnetostriction in Fe-Ni alloy near 30 at% of nickel is associated with the lower or negligible saturation magnetization measured at room temperature.

These alloys are of special interest on account of their scientific and technical importance and the related fact that the magnetostriction becomes very small near to zero as the nickel content of the alloy approaches around 80 at% of nickel of this composition.

6.1   THERMAL EXPANSION MEASUREMENT TECHNIQUE

In thermal expansion measurement, the same setup and procedure as used in magnetostriction experiment is used except that the external magnetic field is kept zero. The fractional change in resistance per nano voltmeter deflection is found to be 2.3×10^{-5}.

6.2   MEASUREMENTS OF THERMAL EXPANSION

The specimen rod along with the specimen holder is hanged from the base of the brass plate and is kept inside a glass tube of length 100 cm and diameter 3.25 cm. The lower end of the glass tube is closed. Liquid nitrogen is poured into the glass cylinder in such a way that the sample holder along with the sample and dummy are dipped in the liquid nitrogen. The temperature of the sample is raised slowly from liquid nitrogen temperature of of 78°K to room temperature. The corresponding change in resistance $\dfrac{dR}{R}$ is recorded by using deflection of the Keithly Nano-voltmeter for the specimen $Fe_{60} Ni_{40}$ This is shown in the fig. (6.2). The temperature of the sample is sensed with a copper-constantan thermocouple and is recorded using a Keithely "Autoranging Microvolt DMM, Model 197A". A calibration curve of the thermocouple used is given in fig.(6.1) The experimental data are shown in Table- (6.1) and the corresponding thermal expansion as a function of temperature is shown in curve (6.2).

Table - 1

6.2   DATA FOR THE THERMAL EXPANSION MEASUREMENT

Thermo-emf in(mV)	Corresponding temperature(°K)	Deflection in nano voltmeter
-5.61	78°	5
-5.60	79°	6
-5.525	83°	10
-5.50	84°	11
-5.46	86°	13
-5.43	88°	15
-5.34	93°	17
-5.25	98°	18
-5.15	103°	19
-5.05	105.5°	20
-5.00	110°	21
-4.93	113°	22
-4.90	114°	23
-4.80	119°	24
-4.70	124°	25
-4.60	128°	27
-4.50	132°	28
-4.40	136°	29
_-4.30_	_140°_	_30_
-4.20	144°	31
-4.08	149°	33
-4.00	152°	34
-3.90	155°	35
-3.80	159°	36
-3.70	163°	37

DATA FOR THE THERMAL EXPANSION MEASUREMENT

Thermo-emf in(mV)	Corresponding temperature(°K)	Deflection in nanovoltmeter
-3.60	167°	39
-3.50	171°	40
-3.40	175°	41
-3.30	178°	43
-3.20	181°	44
-3.10	185°	45
-3.00	188°	47
-2.90	191°	49
-2.80	194°	51
-2.70	197°	52
-2.60	200°	53
-2.50	203°	54
-2.40	206°	55
-2.30	209°	55
-2.20	212°	56
-2.10	215°	57
-1.90	221°	58
-1.80	224°	59
-1.70	227°	60
-1.60	230°	61
-1.50	233°	62

6.3 DATA FOR THE CALIBRATION CURVE FOR COPPER–CONSTANTAN THERMOCOUPLE

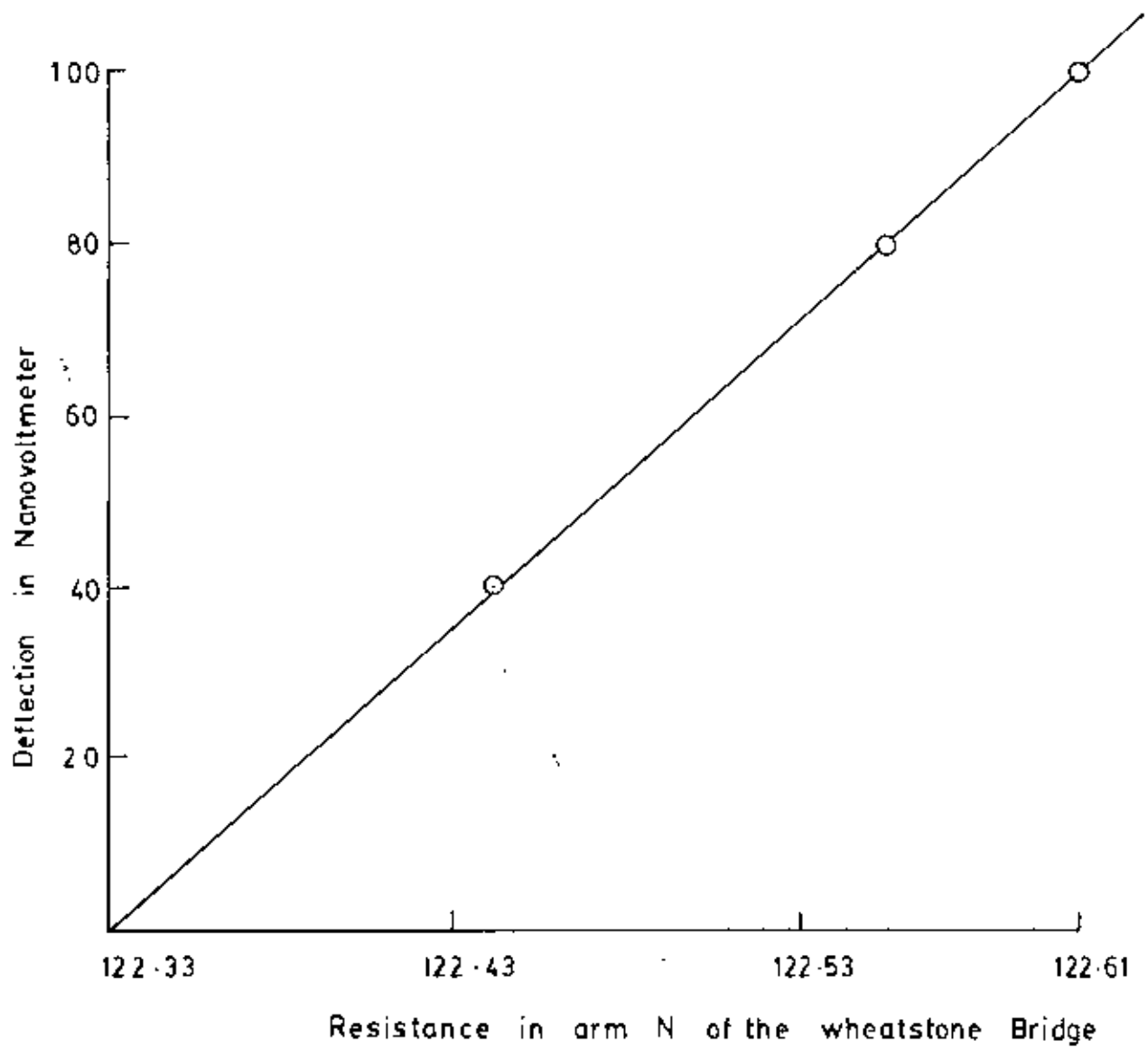| Temperature (°K)	e.m.f. (mV)
77.8	-5.62
83.0	-5.525
93.0	-5.34
103.0	-5.145
113.0	-4.937
123.0	-4.715
133.0	-4.482
143.0	-4.235
153.0	-3.977
163.0	-3.706
173.0	-3.424
183.0	-3.129
193.0	-2.824
203.0	-2.507
213.0	-2.180
223.0	-1.841
233.0	-1.493
243.0	-1.135
253.0	-0.766
263.0	-0.388
273.0	0.000

Fig. 6.3   Deflcetion   against   change   in resistance
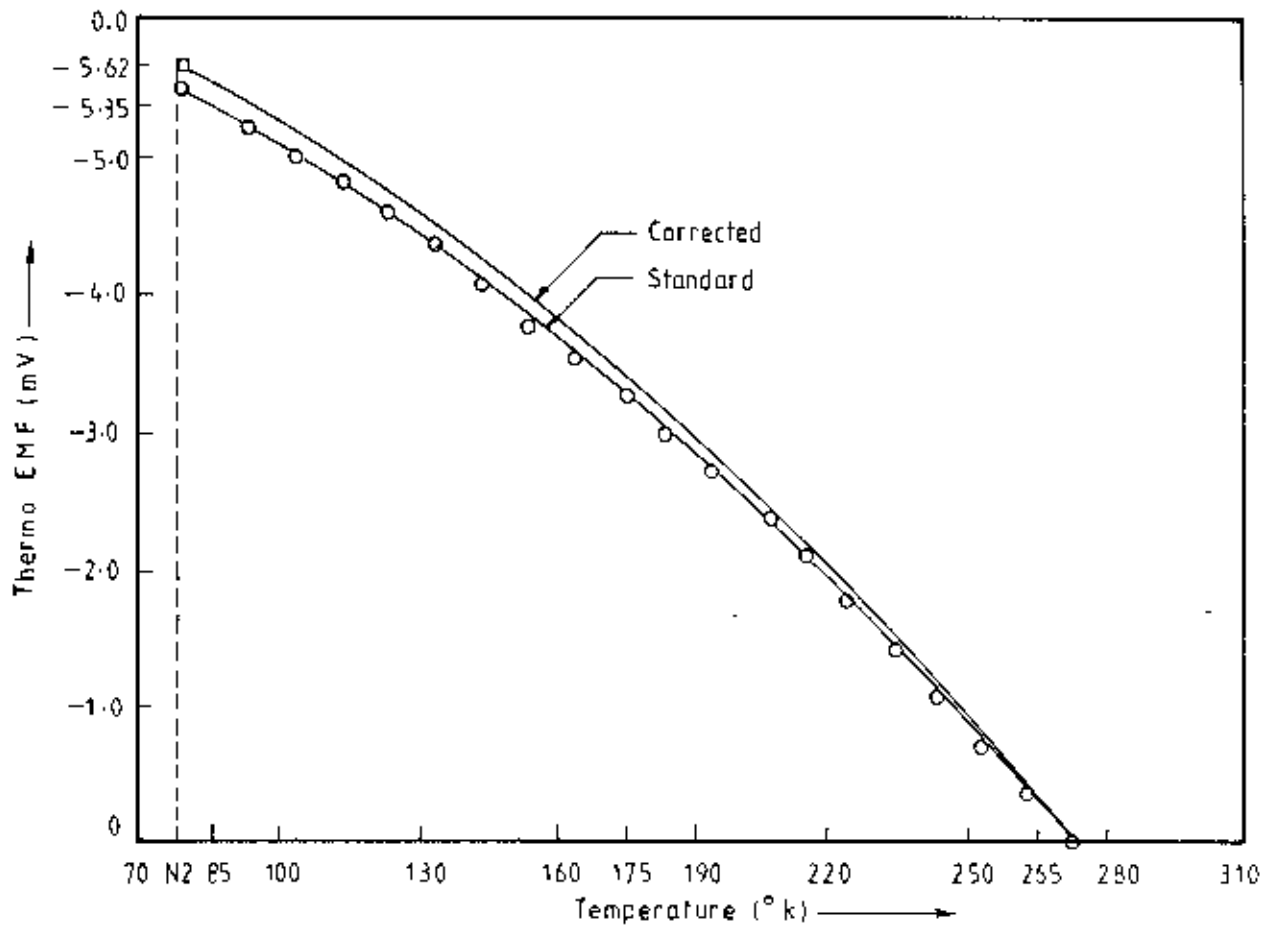
Fig. 6.1: Calibration curve of the Copper – constantan thermocouple

Thermal expension of $Fe_{50}Ni_{50}$ alloy
Gauge factor = 2.09

Fractional change in resistance per
nano voltmeter deflection = 2.3×10^{-5}

Deflection from graph at Temperature, $T_1 = 110°K$	Deflection from graph at Temperature, $T_2 = 230°K$	Difference in deflection	$\dfrac{dR}{R}$	$\dfrac{dl}{l} = \dfrac{1}{\frac{1}{R}dR} \cdot \dfrac{1}{G}$	$\alpha = \dfrac{dl}{l(T_2 - T_1)}$
21	61	40	9.2×10^{-4}	4.4×10^{-4}	3.66×10^{-6}

Fig. 6.2 Thermal expansion measurement curve

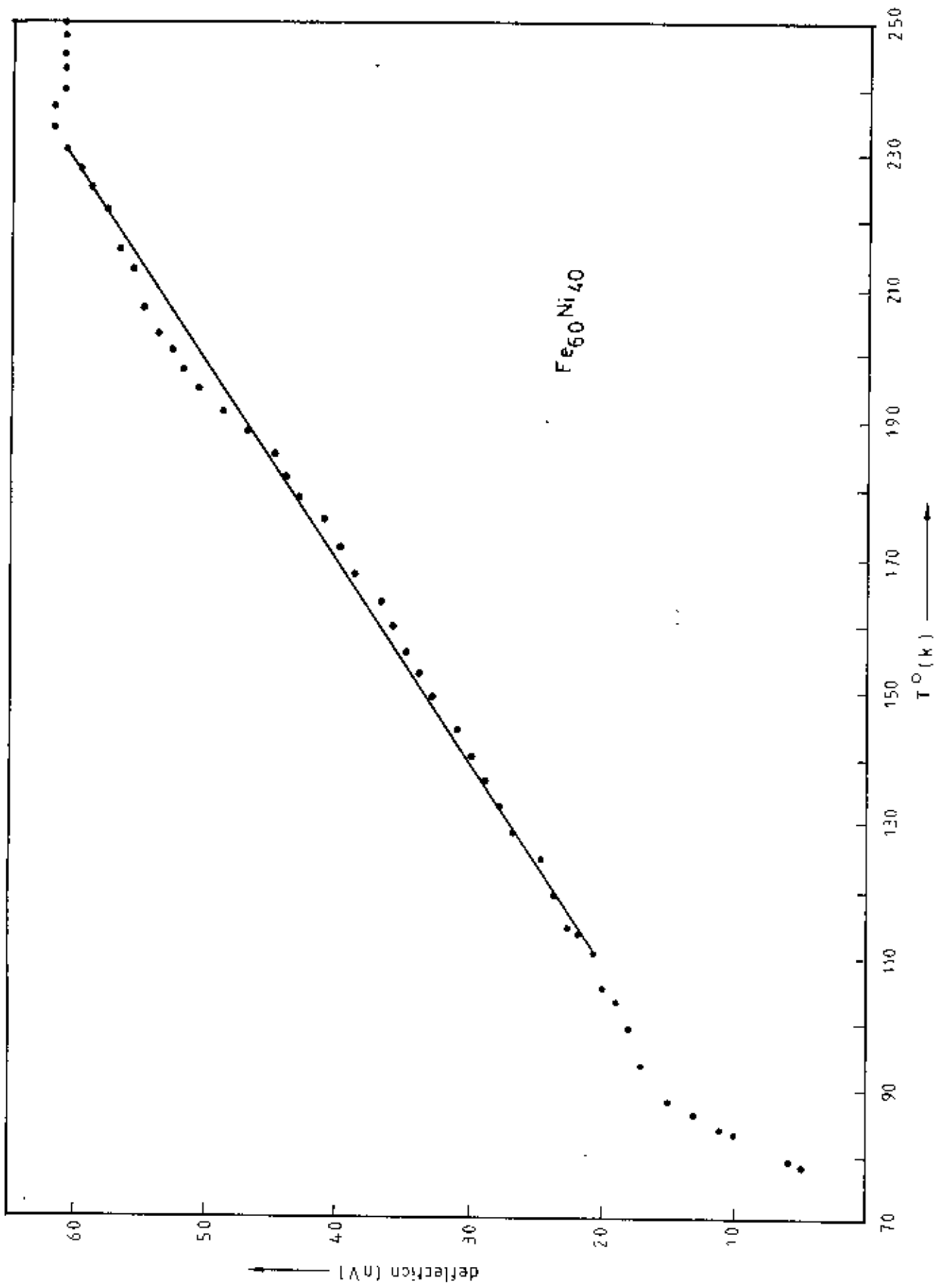## 6.3   RESULT AND DISCUSSION

The fcc Fe-Ni alloys at concentrations around $Fe_{65}Ni_{35}$, show almost constant-invariant-thermal expansion as a function of temperature in a wide range around room temperature (guillame 1897)[6]. According to his results the linear thermal expansion co-efficient α of $Fe_{65}Ni_{35}$ Invar at 300°K is about $1.2 \times 10^{-6} K^{-1}$[1,2], thus an order of magnitude smaller than in the pure components Fe and Ni.

Unusually low thermal expansion was found out from some of the irreversible iron-Nickel alloys and its orgin was investigated as a link of the Invar problem[3,5]

From our experiment we have observed that the thermal expansion of $Fe_{60}Ni_{40}$ is $(3.66) \times 10^{-6}$. For $Fe_{60}Ni_{40}$ alloy composition the apparent near zero thermal expansion co-efficient is explained as follows: In the composition $Fe_{60}Ni_{40}$ and close to this the volume magnetostriction is negative and the thermal expansion co-efficient is positive. Thus volume magnetostriction compensates normal lattice expansion resulting in the near-zero net expansion in a broad temperature renge centered at a room temperature[4]. The specimen used in the present investigation has a composition $Fe_{60}Ni_{40}$ which is close to $Fe_{65}Ni_{35}$. The linear co-efficient of $Fe_{65}Ni_{35}$ measured by C.F. Guillame was $1.2 \times 10^{-6} K^{-1}$[1,2]. Our measured value of α is in good agreement with the value obtained by C.F. Guillame, since both are very close to zero.

Chapter 7   CONCLUSION

Iron-Nickel alloys have been extensively studied as a magnetic material for last one hundred years. But the research in these alloys is still alive both for its numerous applications and due to its complex and interesting magnetic properties. The measurement of magnetization and the study of its variation with magnetic field are important for the understanding and characterization of Fe-Ni alloys. Because the anomalous low thermal expansion of these alloys are due to strong mutual dependence of the magnetic properties and volume magnetostriction. There is an enormous interest in materials with zero thermal expansion and high magnetic permeability due to their technological importance. Although some materials with very low thermal expansion and high magnetic permeability are available commercially, their composition and the preparation techniques are usually not disclosed. There is also a great interest for understanding the mechanism responsible for these unusual properties.

Fe-Ni alloys of the composition $Fe_{100-x}Ni_x$ (when x = 30,35,40,45,50 and 78) are prepared from powders of pure Iron and Nickel. The mixture is then pressed into the required form in a die using a pressing machine. The pressed sample is then sintered at a temperature below the melting points of the constituents. Sintering is essentially a process of bonding solid bodies by atomic forces.

The sintered sample of different compositions of Fe-Ni alloys are annealed at 1000C in a furnace for 15 hours followed by slow cooling. X-ray diffractometer investigation are carried out on these samples to check their status and homogeneity. From the metallographic study the structural characteristics of the Fe-Ni alloys are observed. The present work therefore provide detail practical information about the process of sintering Fe-Ni alloys by powder technique, which is more economic. Since the understanding of the Invar problem is closely related to magnetization and magnetostriction and their dependence on alloy composition, experimental study of these aspects constitute the major part of the present work.

A vibrating sample magnetometer (V.S.M.) is used for measuring magnetization of Fe-Ni alloys, of different compositions. The linear increase of the saturation magnetization in these alloys with iron concentration upto 65 at% is explained by localized model. The sudden decrease of the saturation magnetization in iron nickel alloys around 30 at% Ni is explained as due to negative iron iron nearest neighbour exchange interaction. Both localized model and itinerant electron theory can incorporate this idea.

As the magnetostriction of iron is positive and nickel is negative, it is expected by the thumb rule that in an alloy of these two elements magnetostrictive contributions from these elements will tend to cancell each other. This occurs in our experiments at around 78 at% of nickel. The actual mechanism of magnetostriction being a complex phenomenon due to spin orbit interaction, crystal anisotropy and elastic constants, can not be explained quantitatively. The magnetostriction of the alloys do not show any linearity in respect of the contributions from the constituent elements.

Magnetostriction against magnetization curves provide important information about the domain wall movements during the magnetization process. Initially the magnetization proceeds mostly by the 180 domain wall movements. Magnetostriction increases as we proceed towards the saturation in magnetization. This means that the final process of magnetization is mostly due to 90 domain wall movement.

Thermal expansion of $Fe_{60}Ni_{40}$ alloy is measured using strain gauge technique. Here the volume magnetostriction compensates normal lattice expansion resulting in the near-zero net expansion in a broad temperature range centered at room temperature.

Our measured values of magnetostriction agrees quite well with others works. However, our values of magnetization of the alloy differ for the results of others. This shows that the existing results have some uncertainties and our measurement will contribute towards removing these uncertainties.

REFERENCE

CHAPTER 1

1. Guillaume, Ch.E., C.R. Acad. Sci. 125, (1987), 235
2. Guillaume, Ch.E., C.R. Acad.,Sci. 170, (1920), 1433
3. .Bozorth. R. M. 950, Ferromagnetism (Van Nostrand Princeton).
4. Colling, D. A. and Carr. W. J. journal of Applied Physics, 41 (1970) 5125
5. Collins, M. F. Proc. Phys. Soc. London, 86(1965), 973
6. Crangle, J. and Hallam. G. C. Proc. R. Soc. London, Ser, A272 (1963) 119.
7. Dubinin, S.F., Sidorov S.K. and Valiev E.Z. Physics Status Solidi B46(1971) 337
8. Kondorsky, E.I. and Sedov V.L. J. Appl. Phys. 31(1960) 331
9. Koster, W. and Hofmann, G. Arch. Eisenhue 30(1959) 249
10. Koster, W. and Rauscher, W. Z. Metallkd, 39(1948) 178
11. Koster, W. and Retner, Z. Metallkd 45(1954) 639
12. Kussmann, A. and Rittberg, G. V. Z. Mettallkd 41(1950) 470
13. Koster, W. and Schmidt, W. Arch Eisenhuetenwes, 7(1933) 121
14. Wohlfarth E.P. Phys. Lett. A28(1969) 569
15. Weiss, R. J. Proc. Phys, Soc. London, 82(1963) 281
16. Izuyama, T. and Kubo, R. Journal of Applied Physics, 35(1964) 1074
17. Izuyama, T. and Kubo, R. Journal Applied Physics, 35(1964) 1074
18. Moruzzi, V.L., Phys. Rev. Lett. 57(1986) 2211
19. Krakso, G. L. Phys. Rev. B-36(1987) 8565
20. Ishikawa, Y. and Endoh, Y. J. Phys. Soc. Japan, 23(1967) 205
21. Fujimori, H. J. Phys. Soc. Japan 21(1966), 1860,
22. Kowvel J. S. and Wilson, R. H. J. Appl. Phys. 32(1961) 435
23. Mathon, J., and E. P. Wohlfarth, Phys. Status Solidi 30(1968) K131
24. Kachi, S. and H. Asano, J. Phys. Soc. Japan, 27(1969) 536
25. Kussmann, A. J. Phys. Soc. Japan 17 Suppl B-1(1962) 136
26. Hasegawa, H. and Kanamori, J., J. Phys. Soc. Japan 31(1971) 282
27. Hayase, M., Shiga M. and Nakamura Y., J. Phys. Soc. Japan 30(1971) 729
28. Sidorov, S. K., and Doroshenko, A. V., Phys. Status Solidi 16(1966) 737
29. Menshikov, A. Z., J. Magn. & Magn. Mater, 10 (1979) 205
30. Weiss, P. R. Phys. Rev. 74(1948) 1493

31. Jo, T., J. Phys. Soc. Japan 40(19760) 715

32. Kono Y. and Chikazumi, S. Kabayashi Riken Hakaku 9(1959) 12

33. Kakehashi, Y., Phys. Rev. B-38(1988b) 12051

34. Endoh, Y. and Y. Ishikawa, J. Phys. Soc. Japan 301971) 1614

35. Schlosser. W. F., J. Phys. & Chem. Solids 32(1971) 939

36. Fujimori, H. and Saito, H., J. Phys. Soc. Japan, 20(1065) 293

37. Shiga, M., and Nakamura,Y., J. Phys. Soc. Japan 26 1969) 24

38. Wassermann, J. Magn. & Magn. Mater, 68(1987) 233

39. Wassermann. J. Appl. Phys. 63(1988a) 3921

40. Zahres, Acet. M. H.F., Stamm, W. and Wassermann,E,F., J. Phys. (France) Colloq 49, C 8(1988b) 121

41. Wassermann; in Ferromagnetic Materials Vol. 5,
    Edited by K.H.J. Buschow and E,P. Wohlfarth
    (c) Elsevier Science Publishers B.V., 1990

42. Asgar, M., Ph. D. Thesis, Univesity of Southampton (1970)

43. Slater, J.C., J. Appl. Phys. 8(1937) 385

44. Pauling L.; Phys. Rev. 54 (1938) 899

45. Weiss P.; J. Phys. 6(1907) 661

46. Foner. S.; Rev. Sci, Instr, 27(1956) 548

47. Foner. S. ; Bull. Am. Phys. Soc. Ser. 11.21957) 128

48. Friedel, J., Nuovo Cinento Suppl. vii(1958) 287, J. Phys. Et Rad, 23(1962) 501, 692.

49. Goldman, J.E.; Phys. Rev. 72(1947) 529

50. Shimizu. M., J. Magn. & Magn Matter 10(1979) 231

51. Kanamori, J.; J. Phys. (France) 35(1974) C4, 131

52. Heisenberg. W.; Z Physik 49(1928)619

CHAPTER 2

1. Weiss, P.: J. Phys. 6 (1907) 661

2. Chikazumi, Soshin in Chikazumi. So, Physics of Magnetism, John Wiley & Sons, Inc. Nerw York. London, Sydney.

3. Cullity. B. D.; in Introduction to Magnetic Material.

4. Kouvel.J. S. and Wilson. R. H.: J. Appl. Phys. 32 (1961) 435

5. Heisenberg. W.: Physik. Z. 49 (1928) 619

6. Stoner:E. C. Phil. Mag. [7] 15 (1933) 1080

7. Stoner:E. C. Repts. Progr. Phys 11 (1947) 43

8. Slater: J. C. Phys. Rev. 49 (1936) 537, 981; 52 (1937) 198

9. Krutter: H. Phys. Rev. 48 (1935) 664

10. Koster: G.F. Phys. Rev. 98 (1955) 901

11. Shull.C. G. and Wilkinson: M. K. Phys. Rev. 97 (1955) 304

12. Collins. M. F., Jones, R. V. and Lowde: R. D., J. Phys. Soc. Japan 17, Suppl B-111, (1962) 19

13. Low. G.G.E . and Collins: M. F. J. Appl. Phys. 34 (1963) 1195

14. Friedel: J., Nuova Cimenta Suppl. VII 287 (1958); J. Phys. et Rad. 23 (1962) 501, 692

15. Kondorsky,E. I. and Sedov:V, L., J. Appl. Phys 31S (1960) 331

16. Carr. W. J.; Phys. Rev. 85 (1952) 590   . . . -

17. Hirone. T.; Sci. Rep. Tohoku Univ. 27 (1938) 101

18. Wohlfarth. E. P.; Proc. Roy. Soc. 195A (1949) 434

-19. Zener. C.; Phys. Rev. 81(1951) 446; 82(1951) 403; 83(1951) 299, 85 (1991) 324

20. Slater, J.C., J. Appl. Phys. 8 (1937) 385

21. Pauling, L., Phys. Rev. 54 (1938) 899

22. Neel, L., Ann de Physique 3 (1948) 137

23. Van Vleck.J.H., Phys. Rev. 52 (1938) 1178

24. Kittel.C. and Van Vleck,J. H., Phys. Rev. 118(No. 5)(1960) 1231

25. Asgar, M. A., Proceeding of the international conference on Physics and energy for development, Dhaka, 26-19 January 1985 Page 153

26. Lee. E. W. and Asgar, M. A., Proc. Roy. Soc. 73 (1971) A326

27. Akulov.N. S. and Kondorskiy.Ye. I., Zh. єKsp teor, Fiz. 14(1933) 462

28. Bozorth.R. M.; in Ferromagnetism (Van Nostrand Princeton)

29. Callen.E. and Callen.H. B.; Phys. Rev. B 29 (1963) 10

30. Handley.R.C. O. and Grant.N.J., Proc. Conf. on Rapidly Quenched Metals eds. Steeb.S. and Warlimont.H. (Elsevier, Amsterdam, 1985) P. 1125

31. Fahnle. M. and Egami. T.; J. Appl. Phys. 53 (1982) 2319

32. Cochrane.R. W., Harris.R. and Plischke.J.; J. Non-cryst. Solids 15 (1974) 239.

33. G. Albenga, Atti. Acad. Sci. Torino. C1 fis. mat. mat. 54 (1918/1919) 864

34. Furthmuller. J., Fahnle. M. ; J. of Magnetism and Magnetic Materials, 69 (1987) 79-88

CHAPTER 3

1. Bozorth, R. M. Ferromagnetism (Van Nostrand Princeton).

2. Lakhtin.Y., The phase rule and Equilibrium diagram, Page 95, Engineering Physical Metallurgy. Mir Publishers, Moscow, 1977.

3. Guy. A. G., Elements of Physical Metallurgy, Addision-Wesley Publishing company, Inc. Reading, Massachusetts, U.S.A.

4. Sidney H., Introduction to Physical Metallurgy.

5. Metallographic technique for magnetic materials, Metal Hond Book – 8; Page- 115.

CHAPTER 4

1. Foner.S., Rev. Sci. Instr. 27 (1956) 548

2. Foner.S., Bull. Am. Phys. Soc. Ser 11.2 (1957) 128

3. Foner. S., Rev. Sci. Instr; 30 (1959) 548

4. Mazid. M. A. and Chowdhury.M. A., "Design and Construction of a Foner type Vibrating sample magnetometer", Magnetic material division, AEC, Dhaka.

5. Friedel. J., Nuovo Cimento Suppl. VII (1958) 287,
    J. Phys. et Rad. 23 (1962) 501, 672.

6. Kondorsky, E.I. and V.L. Sedov, J. Appl. Phys. 31 (1960) 331

7. Shull.C. G. and Wilkinson.M. K.; Phys. Rev. 97 (1955) 304.

8. Collins. M. F., Jones. R.V. and Lowde. R.D., J. Phys.Soc. Jadpan 17, Suppl B-III (1962) 19.

9. Low. G.G.E. and Collins. M.F.;
    J. Appl. Phys. 34 (1963) 1195.

10. Carr.W.J., J.Phys. Rev. 85 (1952) 590.

11. Slater. J.C., J. Appl. Phys. 8 (1937) 385

12. Pauling. L., Phys. Rev. 54 (1938) 899 .

13. Mathon and Wohlfarth, Phys. Status Solidi 30 (1968) K131

14. Shiga, M., and Nakamura. Y., J. Phys. Soc. Japan 26 (1969) 24

15. Colling. D. A. and Carr. Jr., J. Appl. Phys. 41 (1970) 5125

16. Kondorski JE TP 10 (1960) 1284

   J. Expt. Pheoret. Phys. (USSR) 37 (1959) 1819

17. Weiss. P. and Foex. G., J. Phys. Radium 1 (1911) 734

18. Physics and Applications of Invar Alloys, Ed. H. Saita, (Maruzen Comp. Let. Tokyo. 1978)

CHAPTER 5

1. Asgar. M. A., Ph.D. Thesis, University of Southampton (1970)

2. Instruction manual; Keithley Instruments Model 140, Precision Nanovolt, DC Amplifier Keithley Instruments, Inc. 28775 Aurora Road, Cleveland and Ohio.

3. Goldman. J.E.; Phys. Rev. 72 (1947) 529

4. Soshin Chikazumi, in Physics of Magnetism. John Wiley & Sons. Inc. New York. London, Sydney

5. Bozorth. R. M.; in Ferromagnetism (Van Nostrand Princeton.

6. Zahres. H., M.Acet, W. Stamm amd E. F. Wassermann, J. of Magnetism and Magnetic Materials 72 (1988) 80–84

7. Sikder. S.S., M.Phil Thesis, BUET

CHAPTER 6

1. Guillaume. C.E., C.R. Acad., Sci; (Paris) 124 (1897) 176.

2. Guillaume. C. E., C. R. Acad. Sci. 170 (1920) 1433.

3. Physics and Applications of Invar Alloys ed H. Saito (Maruzen Comp. Ltd. Tokyo, 1978).

4. Rancourt. D. G., Chehab. S. and Lamarche. G., J. of Magnetism and Mangetic Materials, 78 (1989) 129–152.

5. Yosiaki Tino and Hozumi Kagawa, J. of the Phys.Soc. of Japan, Vol. 28 No. 6, (1970 June) 1445–1451.

6. Wassermann. E. F., in Ferromagnetic Materials Vol. 5, Edited by Buschow. K.H.J. and Wohlfarth. E.P., Elsevier Sci. Publishers B.V. 1990.

7. Lee. E. W. and Asgar. M. A., Phys. Rev. Letters 22 (1969) 1436.